

# การก่อเกิดเชิงพลวัตของเขตศูนย์กลางในควาร์กกลูออนพลาสมา



นายจักรภัทร กรรณิกา

วิทยานิพนธ์นี้เป็นส่วนหนึ่งของการศึกษาตามหลักสูตรปริญญาวิทยาศาสตรมหาบัณฑิต

สาขาวิชาฟิสิกส์

มหาวิทยาลัยเทคโนโลยีสุรนารี

ปีการศึกษา 2557

**DYNAMICAL FORMATION OF CENTER DOMAINS  
IN QUARK-GLUON PLASMA**



**A Thesis Submitted in Partial Fulfillment of the Requirements for the  
Degree of Master of Science in Physics  
Suranaree University of Technology  
Academic Year 2014**

# DYNAMICAL FORMATION OF CENTER DOMAINS IN QUARK-GLUON PLASMA

Suranaree University of Technology has approved this thesis submitted in partial fulfillment of the requirements for a Master's Degree.

Thesis Examining Committee

---

(Prof. Dr. Santi Maensiri)

Chairperson

---

(Asst. Prof. Dr. Ayut Limphirat)

Member (Thesis Advisor)

---

(Dr. Christoph Herold)

Member

---

(Prof. Dr. Yupeng Yan)

Member

---

(Asst. Prof. Dr. Chinorat Kobdaj)

Member

---

(Prof. Dr. Sukit Limpijumnong)

Vice Rector for Academic Affairs  
and Innovation

---

(Prof. Dr. Santi Maensiri)

Dean of Institute of Science

จักรภัทร วรรณิกา: การก่อเกิดเชิงพลวัตของเขตศูนย์กลางในควาร์กกลูออนพลาสมา  
(DYNAMICAL FORMATION OF CENTER DOMAINS IN QUARK-GLUON  
PLASMA) อาจารย์ที่ปรึกษา: ผู้ช่วยศาสตราจารย์ ดร.อายุต ลิ้มพิรัตน์, 64 หน้า

เขตศูนย์กลาง คือ โครงสร้างซึ่งเกิดจากการเสียดสมมาตรของศูนย์กลางในควาร์กกลูออนพลาสมา ซึ่งได้ถูกคาดการณ์โดยการคำนวณแบบแลตทิซคิวซีดี โดยแต่ละเขตของเขตศูนย์กลางถูกจำแนกโดยค่าจำกัดของโพลียาคอฟูลิป ซึ่งในที่นี้มีบทบาทสำคัญในการแยกแยะระหว่างคอนไฟน์และดีคอนไฟน์เฟส เขตศูนย์กลางยังอาจเกิดขึ้นได้ในการชนกันของไอออนหนัก และมีอิทธิพลต่อความหนืดและการไหลเชิงรี ซึ่งเป็นปริมาณที่บ่งถึงการเกิดควาร์กกลูออนพลาสมาในการชนของไอออนหนัก งานวิจัยนี้ได้พัฒนาแบบจำลองพลศาสตร์สำหรับโพลียาคอฟูลิป บนพื้นฐานของแอฟเฟกทีฟโพเทนเชียลและพีโนมิโนโลจิคอลโคเนคติกทอม การศึกษาวิวัฒนาการของโพลียาคอฟูลิป ทำให้สามารถศึกษาการก่อตัวและการสลายของเขตศูนย์กลางในควาร์กกลูออนพลาสมาได้ โดยผลการจำลองในวิทยานิพนธ์นี้ทำให้เกิดความเข้าใจอย่างลึกซึ้ง เกี่ยวกับกระบวนการก่อตัวของเขตศูนย์กลางในระหว่างการชนของไอออนหนัก และช่วยในการทำความเข้าใจเกี่ยวกับขนาดของเขตศูนย์กลาง ซึ่งได้รับอิทธิพลมาจากอุณหภูมิและสัมประสิทธิ์จลน์ในแบบจำลองที่สร้างขึ้น จากงานวิจัย พบว่าการขยายตัวของเขตศูนย์กลางนั้นเกิดขึ้นเนื่องมาจากสัมประสิทธิ์จลน์ และผลจากการคำนวณแบบแลตทิซคิวซีดียังบ่งชี้ให้เห็นว่า ขนาดของเขตศูนย์กลางนั้นขึ้นกับค่าของอุณหภูมิด้วย เช่นเดียวกับผลการคำนวณแบบแลตทิซคิวซีดี ซึ่งสามารถกำหนดค่าของสัมประสิทธิ์จลน์ให้อยู่ในรูปของอุณหภูมิ โดยทำยู่สุดพบว่า การก่อตัวของเขตศูนย์กลางนั้นอยู่ในช่วงชีวิตของควาร์กกลูออนพลาสมาที่พลังงานของแอลเอชซี โดยการคำนวณที่เกี่ยวข้องกับผลกระทบของเขตศูนย์กลางจะถูกพิจารณาในงานวิจัยในอนาคต

สาขาวิชาฟิสิกส์  
ปีการศึกษา 2557

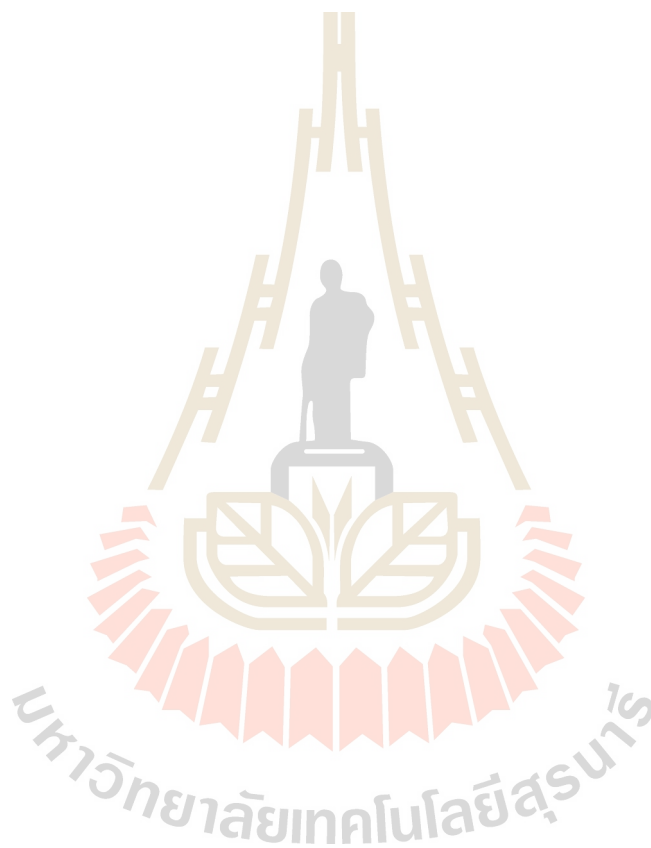
ลายมือชื่อนักศึกษา \_\_\_\_\_  
ลายมือชื่ออาจารย์ที่ปรึกษา \_\_\_\_\_  
ลายมือชื่ออาจารย์ที่ปรึกษาร่วม \_\_\_\_\_

JAKAPAT KANNIKA : DYNAMICAL FORMATION OF CENTER DOMAINS  
IN QUARK-GLUON PLASMA. THESIS ADVISOR : ASST. PROF. AYUT  
LIMPHIRAT, Ph.D. 64 PP.

QUARK-GLUON PLASMA/CENTER DOMAINS/HEAVY-ION COLLISIONS/ DY-  
NAMIC SYMMETRY BREAKING

Center domains are structures based on spontaneous breakdown of center symmetry as expected in quark-gluon plasma (QGP) from lattice QCD calculations. Each domain is characterized by a finite value of the Polyakov loop, which here serves as an order parameter to distinguish between confined and deconfined phase. Center domains might possibly occur in heavy-ion collision and may have influence on observable like viscosity or elliptic flow. In this work, we develop a fully dynamical model for the Polyakov loop based on an effective potential and a phenomenological kinetic term. Studying the time evolution of the Polyakov loop allows us to study formation and decay of center domains in the QGP. The results of this simulation give us insight into the formation procedure during a heavy-ion collision and help us understand how the domain size is influenced by temperature and the kinetic coefficient in our model. We find that the domain size grows with this coefficient, together with recent data from lattice QCD, where the domain size was calculated as a function of temperature, we can fix the value of the kinetic coefficient as a function of temperature. Finally, we determine the formation time of domains and find it within the lifetime of a QGP at LHC energies,

therefore making the formation of center domains a relevant effect that needs to be considered in future calculations.



School of Physics

Student's Signature \_\_\_\_\_

Academic Year 2014

Advisor's Signature \_\_\_\_\_

Co-Advisor's Signature \_\_\_\_\_

## ACKNOWLEDGEMENTS

Firstly, I would like to express my gratitude to all people who have supported, assisted and taught me which later influenced me to complete my thesis.

I would like to thank Prof. Dr. Yupeng Yan for giving me a chance to join the Nuclear and Particle Physics group and teaching me several courses involving particle physics. And I would like to thank Asst. Prof. Dr. Chinorat Kobdaj for encouraging me to keep studying and doing research in the field of particle physics, without you, I would not have finished my master degree in physics. Thank you Asst. Prof. Dr. Ayut Limpirat for supporting me all along and for being my thesis advisor who always gave me very useful advice. And thank you Dr. Christoph Herold for teaching me physics and training me to do research.

Finally, I would like to express my deepest gratitude to my parents for giving me the freedom to think, to work and even to play.

Jakapat Kannika

# CONTENTS

	<b>Page</b>
ABSTRACT IN THAI . . . . .	I
ABSTRACT IN ENGLISH . . . . .	II
ACKNOWLEDGEMENTS . . . . .	IV
CONTENTS . . . . .	V
LIST OF TABLES . . . . .	VII
LIST OF FIGURES . . . . .	VIII
<b>CHAPTER</b>	
<b>I INTRODUCTION . . . . .</b>	<b>1</b>
<b>II POLYAKOV LOOP POTENTIAL . . . . .</b>	<b>6</b>
2.1 Polyakov loop potential . . . . .	6
2.2 Thermodynamic properties . . . . .	8
<b>III EQUATIONS OF MOTION . . . . .</b>	<b>13</b>
<b>IV SIMULATION METHOD . . . . .</b>	<b>18</b>
4.1 Numerical implementation . . . . .	18
4.2 Numerical parameters . . . . .	20
4.3 Initial conditions . . . . .	20
4.4 Fixing sigma . . . . .	21
4.5 Tracking evolution of center domains . . . . .	24

## CONTENTS (Continued)

	<b>Page</b>
<b>V     RESULTS</b> . . . . .	<b>25</b>
5.1 Sigma coefficient . . . . .	25
5.2 Formation of center domains . . . . .	28
5.3 Decay of center domains . . . . .	34
<b>VI    CONCLUSIONS AND DISCUSSIONS</b> . . . . .	<b>43</b>
REFERENCES . . . . .	45
APPENDICES	
APPENDIX A RESEARCH WORKFLOW . . . . .	51
APPENDIX B NATURAL UNITS . . . . .	52
APPENDIX C CODE IMPLEMENTATIONS . . . . .	54
CURRICULUM VITAE . . . . .	64

## LIST OF TABLES

Table	Page
4.1 Numerical parameters. . . . .	20
B.1 Natural units in particle physics. . . . .	53



# LIST OF FIGURES

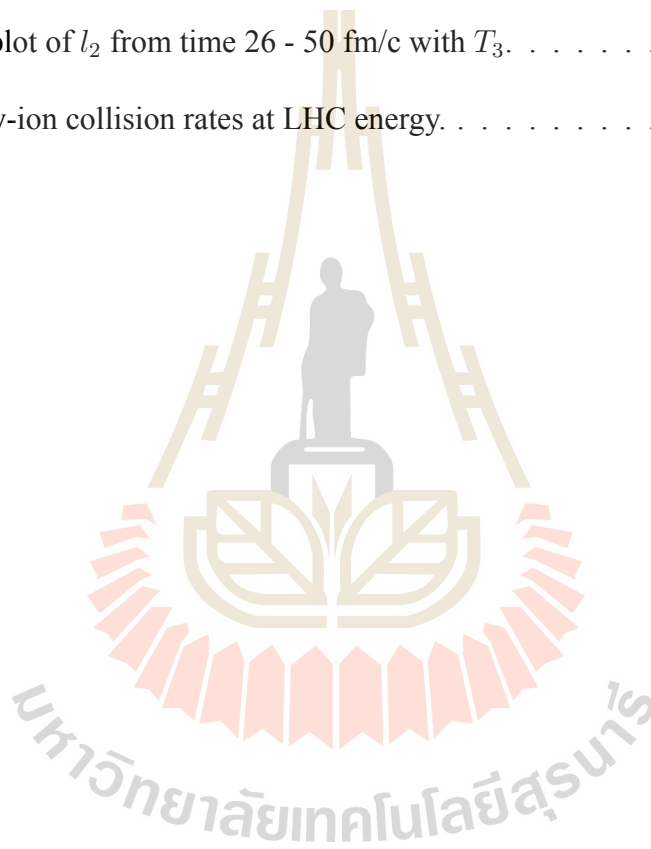
<b>Figure</b>		<b>Page</b>
1.1	Illustrations of atoms and molecules from John Dalton’s book, “A New System of Chemical Philosophy (1808)” . . . . .	2
1.2	Standard model of elementary particles shows various particles that have been observed so far, figure by MissMJ, used under CC BY 3.0. . . . .	3
1.3	Schematic of center domains where $\nu = 0$ , $\nu = 1$ and $\nu = 2$ are different in types of domains, from (Asakawa et al., 2013). . . . .	5
2.1	Contour plot of Polyakov loop potential at $T = 100$ MeV. . . . .	7
2.2	Contour plot of Polyakov loop potential at $T = 300$ MeV. . . . .	8
2.3	Contour plot of Polyakov loop potential at $T = 500$ MeV. . . . .	8
2.4	Minimum point of the Polyakov loop potential as a function of $T$ . . . . .	10
2.5	Absolute value of the Polyakov loop in the equilibrium as a function of $T$ . . . . .	10
2.6	Pressure of the Polyakov loop potential as a function of $T$ . . . . .	11
2.7	Entropy of the Polyakov loop potential as a function of $T$ . . . . .	11
2.8	Free energy of a heavy static quark as a function of $T$ . . . . .	12
2.9	Energy density of the Polyakov loop potential as a function of $T$ . . . . .	12
4.1	Small fluctuations in Polyakov loop at $z = 0$ fm and time $t = 0.005$ fm/c. . . . .	21
4.2	Space-time lattices with a different sigma values. . . . .	22

## LIST OF FIGURES (Continued)

Figure	Page
4.3	Average diameter of domains for two resolution scales, (Borsanyi et al., 2011). . . . . 23
5.1	Exponential fit of the correlation function for $T = 283.5$ MeV. . . . . 25
5.2	Exponential fit of the correlation function for $T = 297.0$ MeV. . . . . 26
5.3	Exponential fit of the correlation function for $T = 310.5$ MeV. . . . . 27
5.4	Sigma as a function of temperature. . . . . 27
5.5	Evolution of standard deviation from time 0 - 25 fm/c with $T_1$ . . . . . 28
5.6	Evolution of standard deviation from time 0 - 25 fm/c with $T_2$ . . . . . 29
5.7	Evolution of standard deviation from time 0 - 25 fm/c with $T_3$ . . . . . 29
5.8	Evolution of standard deviation from time 0 - 25 fm/c with $T_1, T_2$ and $T_3$ . 30
5.9	Plan plot of $l_2$ from time 0 - 25 fm/c with $T_1$ . . . . . 31
5.10	Plan plot of $l_2$ from time 0 - 25 fm/c with $T_2$ . . . . . 32
5.11	Plan plot of $l_2$ from time 0 - 25 fm/c with $T_3$ . . . . . 33
5.12	Evolution of standard deviation from time 26 - 50 fm/c with $T_1$ . . . . . 34
5.13	Evolution of standard deviation from time 26 - 50 fm/c with $T_2$ . . . . . 35
5.14	Evolution of standard deviation from time 26 - 50 fm/c with $T_3$ . . . . . 35
5.15	Evolution of standard deviation from time 26 - 50 fm/c with $T_1, T_2$ and $T_3$ 36
5.16	Plan plot of $l_2$ from time 26 - 50 fm/c with $T_1$ . . . . . 37
5.17	Plan plot of $l_2$ from time 26 - 50 fm/c with $T_1$ . . . . . 38
5.18	Plan plot of $l_2$ from time 26 - 50 fm/c with $T_2$ . . . . . 39

## LIST OF FIGURES (Continued)

<b>Figure</b>		<b>Page</b>
5.19	Plan plot of $l_2$ from time 26 - 50 fm/c with $T_2$ . . . . .	40
5.20	Plan plot of $l_2$ from time 26 - 50 fm/c with $T_3$ . . . . .	41
5.21	Plan plot of $l_2$ from time 26 - 50 fm/c with $T_3$ . . . . .	42
6.1	Heavy-ion collision rates at LHC energy. . . . .	44



# CHAPTER I

## INTRODUCTION

In the past, people believed that all elements in nature were composed of indivisible particles called *atoms*. The first group of people who considered the concept of an atom were ancient Greek and Indian philosophers, studying so-called *Atomism*. Atomism comprises the idea that all elements in nature consist of atoms and voids. However, the crucial problem of Atomism was the lack of experimental evidence. Note that, in modern science, any theory requires experimental support to be verified. In the 19<sup>th</sup> century, the study of atoms became famous again under the name of *Atomic Theory*. This Atomic Theory was developed by John Dalton, an English chemist, physicist and meteorologist, see figure 1.1. The origin of the theory was not well understood. However, the theory was later verified by many experimental results from other works. The idea of his theory can be summarized in four statements:

1. All elements in nature are made of atoms where one atom is indivisible and indestructible,
2. Any single element is composed of atoms which are identical in size, mass and other properties, different elements have different types of atoms,
3. Any two or more elements can form chemical compounds with an integer ratio,
4. A chemical reaction is a rearrangement of atoms.

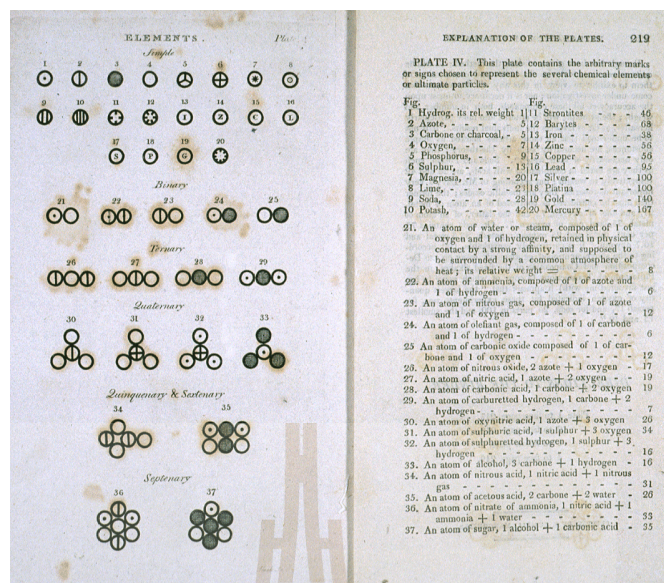


**Figure 1.1** Illustrations of atoms and molecules from John Dalton's book, "A New System of Chemical Philosophy (1808)".

This was the first time when scientists had gained an empirical understanding about matter. So, with this success, the Atomic Theory of Dalton is considered as a foundation of particle physics and another related fields in a few centuries later.

Later, contrary to some ideas of the Atomic Theory of Dalton, physicists found that atoms are not indivisible, but contain smaller particles such as electrons, protons and neutrons. Moreover, from modern particle physics, we know that even protons and neutrons are composed of smaller particles called quarks, see figure 1.2 for a table of elementary particles as they are known today.

After the Big Bang, our universe started to expand and cool, resulting in several phases and phase changes to the contained matter. All those phases have different thermodynamic properties. In this work, we focus on one of the early phases called *quark-gluon plasma (QGP)*. The QGP is a primordial state of matter created at about

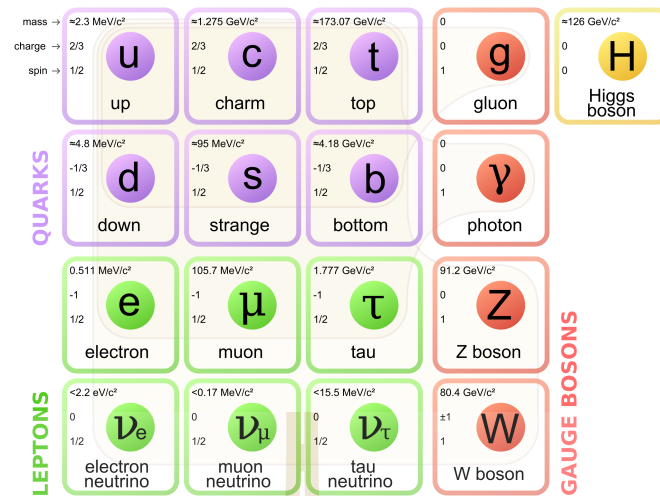


**Figure 1.2** Standard model of elementary particles shows various particles that have been observed so far, figure by MissMJ, used under CC BY 3.0.

$10^{-5}$  s after the Big Bang, The term of QGP denotes matter composed of two elementary particles:

*Quarks*, which are considered as fundamental constituents of matter.

*Gluons*, which act as carriers of the strong nuclear force between quarks.

From the QGP phase, hadrons emerged after further cooling, later atomic nuclei, atoms, and finally gravitating large-scale structures such as stars and galaxies. In the QGP phase, quarks and gluons are in no bound state under the extremely hot and dense conditions. The theory describing the interaction of quarks and gluons due to so called color charges (red (R), green (G) and blue (B)) is *Quantum Chromodynamics (QCD)* which was first proposed by Nambu in 1966. One remarkable feature of QCD which distinguishes hadronic matter from a QGP is called *confinement*. In confinement, quarks are bound together in color-neutral particles such as baryons and mesons. Baryons are composite particles made up of three quarks e.g. protons (p), neutrons (n). Mesons are

composite particles made up of one quark and one antiquark e.g. pions ( $\pi$ ), kaons (K). In contrast to that, in QGP the relevant degrees of freedom carry color charge, matter is deconfined. Nevertheless, isolated color charges have never been observed experimentally. Another characteristic property that distinguishes the QGP from the hadron gas is the restoration of chiral symmetry at high temperatures. The QGP can be found or created in 1) The early universe at about  $10^{-5}$  s after the Big Bang, 2) Superdense stars such as neutron stars or quark stars, 3) Heavy-ion collisions.

Nowadays, heavy-ion collisions are done by colliding two heavy nuclei at ultra-relativistic energies using large accelerator facilities. At the moment such experiments are performed at the Relativistic Heavy Ion Collider (RHIC) at Brookhaven National Laboratory and the Large Hadron Collider (LHC) at CERN. At RHIC, scientists found evidence for the formation of a strongly interacting quark-gluon plasma (sQGP) (Arsene et al., 2005; Adcox et al., 2005; Back et al., 2005; Adams et al., 2005; Gyulassy and McLerran, 2005; Müller and Nagle, 2006), based on the discoveries of 1) Elliptic Flow 2) Low ratio of shear viscosity to entropy density  $\eta/s$  3) Jet quenching. These evidences show that the sQGP behaves rather like an ideal fluid than a gas of non-interacting particles.

From lattice QCD studies (Danzer et al., 2010; Borsanyi et al., 2011), the existence of so called *center domains* was confirmed. Center domains are structures that have recently claimed to be responsible for some crucial properties of QGP (Asakawa et al., 2013). In (Asakawa et al., 2013), the authors argue that two important properties of QGP, low shear viscosity and jet quenching can be explained by the formation of center domains in the QGP. This was our motivation to study the behavior and dynamics

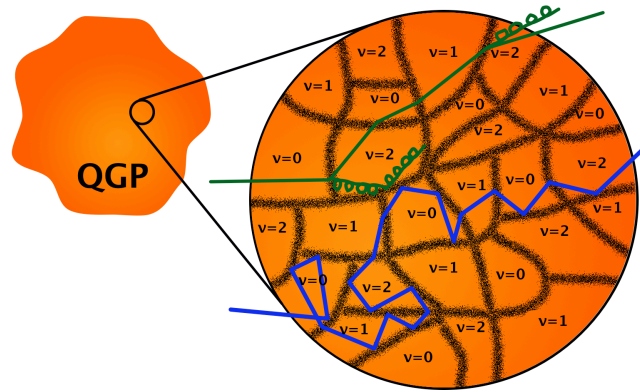


**Figure 1.3** Schematic of center domains where  $\nu = 0$ ,  $\nu = 1$  and  $\nu = 2$  are different in types of domains, from (Asakawa et al., 2013).

of center domains in QGP. In (Asakawa et al., 2013), it is argued that domain walls act as potential barriers for in-medium particles, thus limiting their free wavelength, which accounts for a small value of  $\eta/s$ . On the other hand, jets may rapidly lose their energy in the medium via interaction with the walls and subsequent radiation of soft gluons, see figure 1.3.

Our research here focuses on developing a dynamical model for an effective Polyakov loop field in a QGP. We use a phenomenological Lagrangian from a Polyakov loop potential and a phenomenological kinetic term. Then we study the evolution of the Polyakov loop field in (3+1) dimensions. We hereby restrict ourselves to the case of a medium with a homogeneous temperature. We expect to be able to observe the formation of center domains after changing the global temperature from below to above the critical temperature  $T_c$ . Our goal is to give estimates for the formation and decay time of domains to better understand their possible role in heavy-ion collisions.

## CHAPTER II

### POLYAKOV LOOP POTENTIAL

Center domains occur due to the spontaneous breakdown of center symmetry  $Z(3) \subset SU(3)$  at high temperatures. Therefore, the existence of center domains is expected in a QGP phase. In QCD, one way to distinguish between QGP phase and hadronic phase is using confinement. Confinement can be mathematically described by the *Polyakov loop* potential. The Polyakov loop arises from pure  $SU(3)$  gauge theory, where it serves as an order parameter which distinguishes between a center symmetric confined phase and a deconfined phase where this symmetry is broken.

#### 2.1 Polyakov loop potential

The fundamental Polyakov loop is defined as

$$L(\vec{x}) = \frac{1}{3} \text{tr} \text{P exp} \left[ ig \int_0^{1/T} A_4(\tau, \vec{x}) d\tau \right], \quad (2.1)$$

where  $P$  denotes the path-ordering operator,  $g$  is the strong coupling constant,  $T$  is the temperature and  $A_4$  is the temporal component of a static gluon background field in Euclidean space-time. From fits of lattice QCD data (Boyd et al., 1996) in the pure gluon sector, we obtain a potential for the Polyakov loop (Roessner et al., 2007)

$$U(L) = -bT[54e^{-a/T} |L|^2 + \ln P(L, L^\dagger)], \quad (2.2)$$

where  $L$  is the Polyakov loop,  $T$  is the temperature,  $a = 0.664 \text{ GeV}$ ,  $b = 0.0075 \text{ GeV}^3$  and  $P(z, \bar{z}) = 1 - 6|z|^2 - 3|z|^4 + 4(z^3 + \bar{z}^3)$ . Figures 2.1 to 2.3 show plots of the Polyakov

loop potential in the complex plane  $L = l_1 + il_2$  with temperatures  $T = 100$  MeV,  $T = 300$  MeV and  $T = 500$  MeV respectively. The equilibrium point of the potential is shifted from one point in figure 2.1 to three points in figure 2.3, due to the spontaneous breakdown of center symmetry  $Z(3)$  at the critical temperature of  $T = T_c = 270$  MeV. Effective potentials for the Polyakov loop are often used in low-energy models such as the Polyakov loop Nambu-Jona-Lasinio (PNJL) model (Fukushima, 2004) or the Polyakov-Quark-Meson (PQM) model (Schaefer et al., 2007; Herbst et al., 2011). In pure gauge theory, the Polyakov loop is related to the free energy of an infinitely heavy static quark  $F_Q(T)$  by

$$F_Q(\vec{x}, T) = -T \ln |\langle L(\vec{x}, T) \rangle|, \quad (2.3)$$

where

**In confinement:**  $F_Q$  is infinite,  $\langle L \rangle = 0$ ,

**In deconfinement:**  $F_Q$  is finite,  $\langle L \rangle > 0$ .

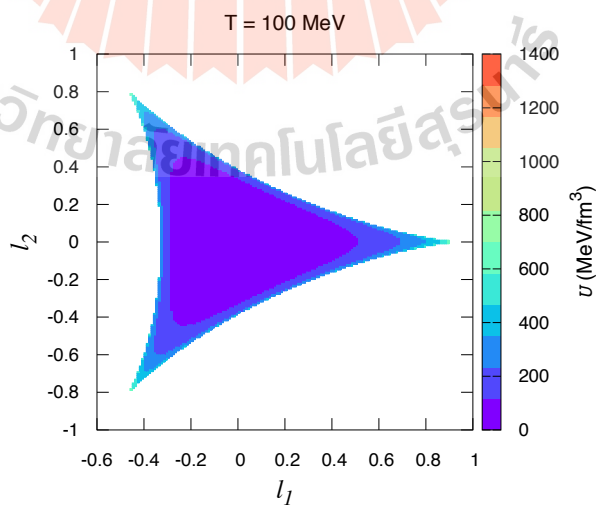


**Figure 2.1** Contour plot of Polyakov loop potential at  $T = 100$  MeV.

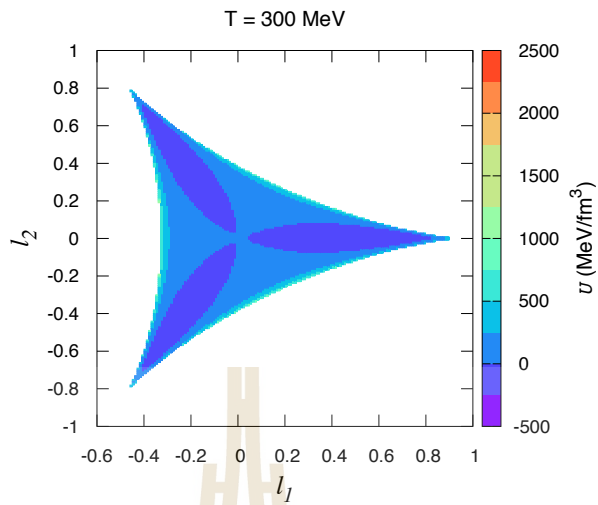


**Figure 2.2** Contour plot of Polyakov loop potential at  $T = 300$  MeV.

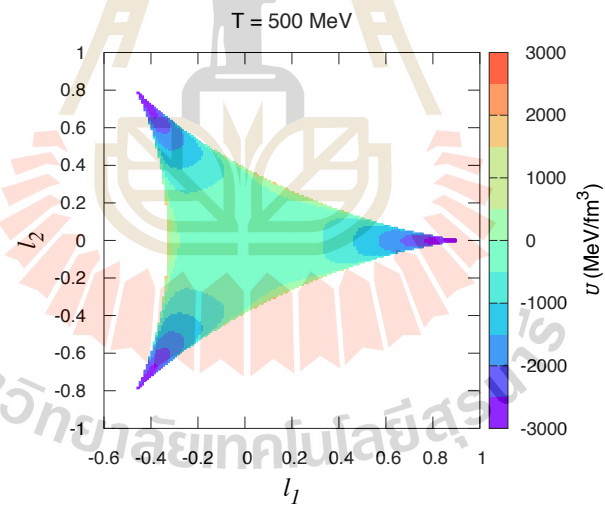


**Figure 2.3** Contour plot of Polyakov loop potential at  $T = 500$  MeV.

## 2.2 Thermodynamic properties

From equations (2.2) and (2.3), we can study thermodynamic properties of pure gluon QCD, such as pressure, energy density, entropy density and free energy density of

test quarks as a function of temperature. By this, we can understand the consistency of the Polyakov loop potential with pure gauge QCD. We will therefore also see that there is a first-order phase transition from the Polyakov loop potential. However, from lattice QCD we know that there is no phase transition for zero chemical potential, but rather an analytic crossover (Aoki et al., 2006). We might expect a first-order phase transition for high density or chemical potential (Scavenius et al., 2001; Schaefer and Wambach, 2005).

In figure 2.4, we track a minimum point of the Polyakov loop potential under the transition from  $T = 0$  MeV to  $T = 500$  MeV. Above the critical temperature  $T_c$ , there are three degenerate ground states according to three minima in the potential. The absolute value of the Polyakov loop in figure 2.5 is able to identify the phase of our system, where in the confined phase  $L$  equals 0 and in the deconfined phase ranges from about 0.5 to 1.0. From the data in figures 2.4 and 2.5, we can further find the pressure as the negative value of the potential, see figure 2.6, the entropy density which is the derivative of the pressure with respect to temperature, see figure 2.7, the free energy of a heavy static quark according to equation (2.3), see figure 2.8 and finally, the energy density which can be found from the relation  $e = Ts - p$ , see figure 2.9.

From these plots we can clearly identify  $T_c$  at 270 MeV from the kink in the pressure and the discontinuity in  $L$ ,  $s$  and  $e$  as functions of  $T$ .

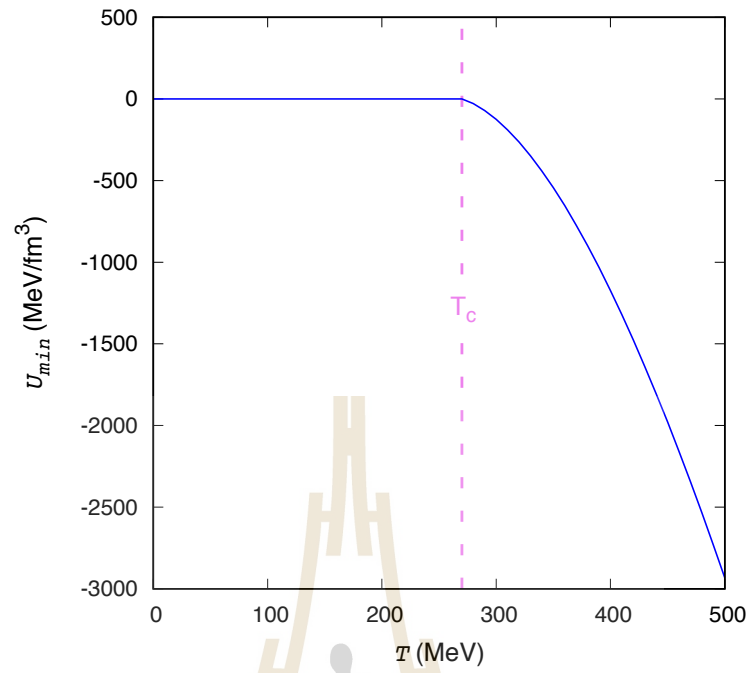


**Figure 2.4** Minimum point of the Polyakov loop potential as a function of  $T$ .

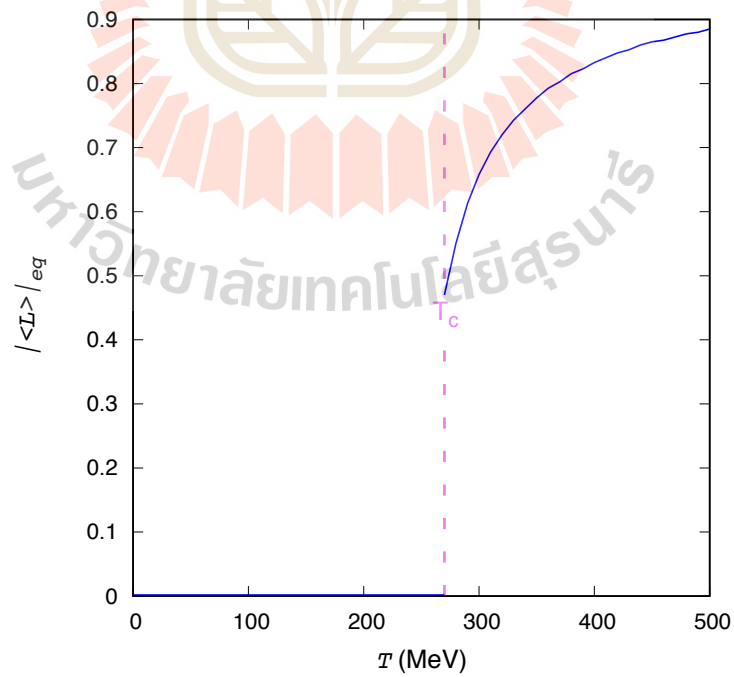


**Figure 2.5** Absolute value of the Polyakov loop in the equilibrium as a function of  $T$ .

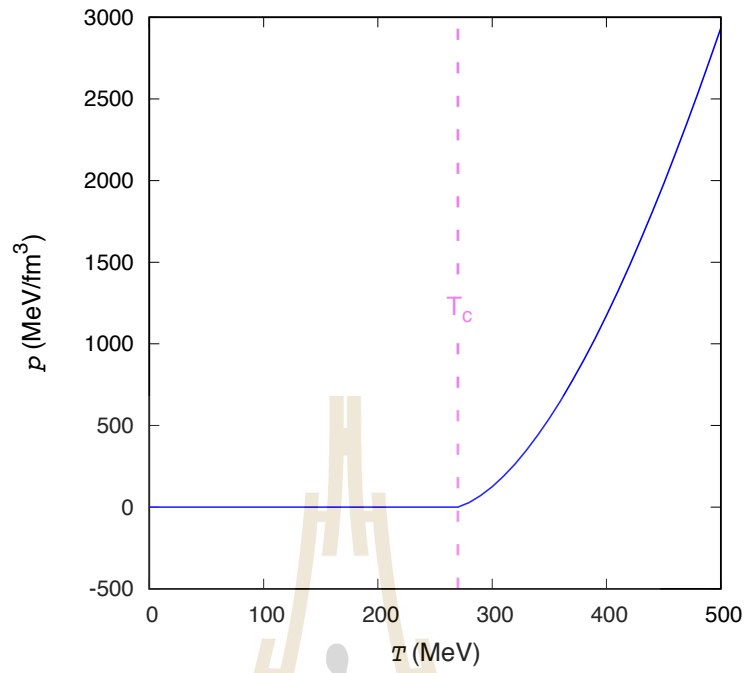


**Figure 2.6** Pressure of the Polyakov loop potential as a function of  $T$ .

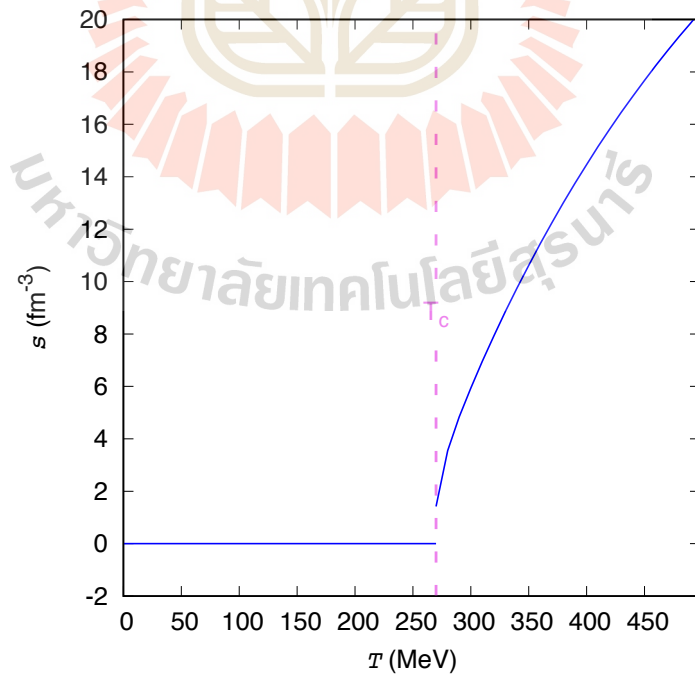


**Figure 2.7** Entropy of the Polyakov loop potential as a function of  $T$ .

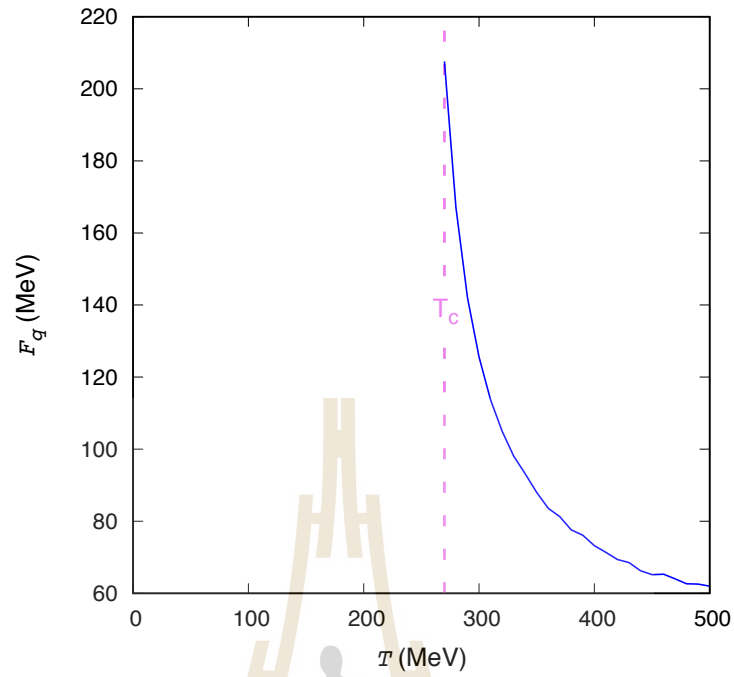


**Figure 2.8** Free energy of a heavy static quark as a function of  $T$ .

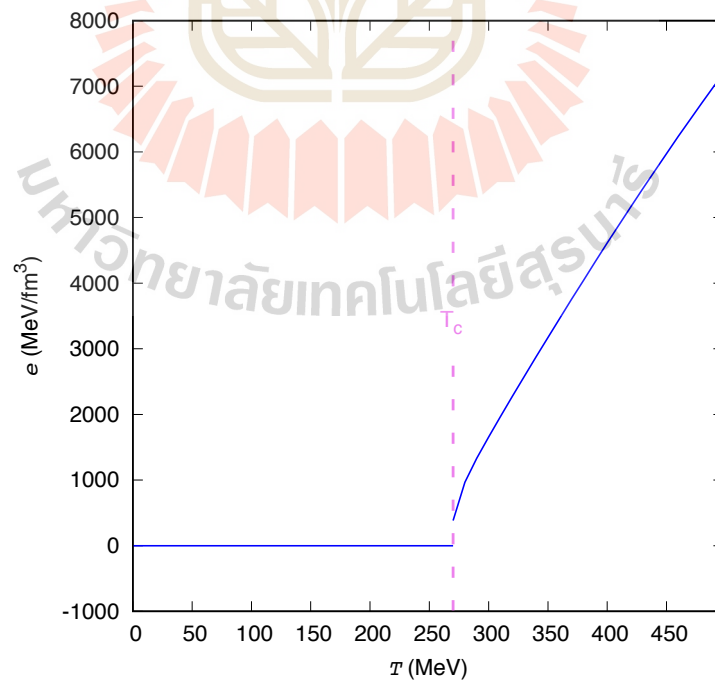


**Figure 2.9** Energy density of the Polyakov loop potential as a function of  $T$ .

## CHAPTER III

### EQUATIONS OF MOTION

Our goal is to study the dynamics of center domains in QGP via the Polyakov loop. As the Polyakov loop has no explicit time dependence, we have to pursue a phenomenological ansatz similar to what has been proposed in (Dumitru and Pisarski, 2001; Herold et al., 2013; Fraga et al., 2007) to study its dynamics. We write down the Lagrangian density as

$$\mathcal{L} = \frac{\sigma}{2} T^2 \partial_\mu L \partial^\mu \bar{L} - U(L, \bar{L}), \quad (3.1)$$

where  $\sigma$  is a dimensionless parameter playing the role of a surface tension that we have to determine later by comparison with the domain size from lattice QCD data (Borsanyi et al., 2011). Splitting the complex-valued Polyakov loop into its imaginary and real part  $L = l_1 + il_2$  and  $\bar{L} = l_1 - il_2$ , equation (2.2) becomes

$$\begin{aligned} U(l_1 + il_2) &= -bT[54e^{-a/T} |l_1 + il_2|^2 + \ln P(l_1 + il_2, (l_1 + il_2)^\dagger)] \\ &= -bT[54e^{-a/T} (l_1^2 + l_2^2) + \ln P(l_1 + il_2, l_1 - il_2)]. \end{aligned} \quad (3.2)$$

For the polynomial function  $P$  we obtain

$$\begin{aligned} P(l_1 + il_2, l_1 - il_2) &= 1 - 6 |l_1 + il_2|^2 - 3 |l_1 + il_2|^4 + 4((l_1 + il_2)^3 + (l_1 - il_2)^3) \\ &= 1 - 6(l_1^2 + l_2^2) - 3(l_1^2 + l_2^2)^2 + 4(l_1^3 + 3il_1^2 l_2 - 3l_1 l_2^2 + l_2^3) \\ &\quad + 4(l_1^3 - 3il_1^2 l_2 - 3l_1 l_2^2 - l_2^3) \\ &= 1 - 6(l_1^2 + l_2^2) - 3(l_1^2 + l_2^2)^2 + 4(2l_1^3 - 6l_1 l_2^2). \end{aligned}$$

In equation (3.1)  $\partial_\mu L \partial^\mu \bar{L}$  can be written as

$$\begin{aligned}\partial_\mu L \partial^\mu \bar{L} &= \partial_\mu (l_1 + il_2) \partial^\mu (l_1 - il_2) \\ &= (\partial_\mu l_1 + i \partial_\mu l_2) (\partial^\mu l_1 - i \partial^\mu l_2) \\ &= \partial_\mu l_1 \partial^\mu l_1 + \partial_\mu l_2 \partial^\mu l_2.\end{aligned}\tag{3.3}$$

From the general Euler–Lagrange equation:

$$\partial_\mu \left( \frac{\partial \mathcal{L}}{\partial (\partial_\mu \phi)} \right) - \frac{\partial \mathcal{L}}{\partial \phi} = 0,\tag{3.4}$$

and equation (3.3), we have the first Euler–Lagrange equation for the real part of the Polyakov loop

$$\frac{\partial}{\partial x^\mu} \frac{\partial \mathcal{L}}{\partial (\partial_\mu l_1)} = \frac{\partial \mathcal{L}}{\partial l_1},\tag{3.5}$$

and the second Euler–Lagrange equation for the imaginary-part of the Polyakov loop

$$\frac{\partial}{\partial x^\mu} \frac{\partial \mathcal{L}}{\partial (\partial_\mu l_2)} = \frac{\partial \mathcal{L}}{\partial l_2}.\tag{3.6}$$

From the Euler-Lagrange equations (3.5) and (3.6), the phenomenological Lagrangian (3.1) and the complex valued Polyakov loop potential (3.2), we can now find the equations of motion. We begin with the equation of motion for the real part of the Polyakov loop  $l_1$

$$\begin{aligned}
\frac{\partial \mathcal{L}}{\partial l_1} &= \frac{\partial}{\partial l_1} \left[ \frac{\sigma}{2} T^2 (\partial_\mu l_1 \partial^\mu l_1 + \partial_\mu l_2 \partial^\mu l_2) - U(l_1, l_2) \right] \\
&= \frac{\partial}{\partial l_1} U(l_1, l_2) \\
&= \frac{\partial}{\partial l_1} \left[ -bT [54e^{-a/T} (l_1^2 + il_2^2) + \ln P(l_1 + il_2, l_1 - il_2)] \right] \\
&= -108bTe^{-a/T} l_1 + \left[ \frac{1}{P(l_1 + il_2, l_1 - il_2)} \frac{\partial}{\partial l_1} P(l_1 + il_2, l_1 - il_2) \right] \\
&= -108bTe^{-a/T} l_1 + \left[ \frac{1}{P(l_1 + il_2, l_1 - il_2)} \frac{\partial}{\partial l_1} (1 - 6(l_1^2 + l_2^2) \right. \\
&\quad \left. - 3(l_1^2 + l_2^2)^2 + 4(2l_1^3 - 6l_1 l_2^2)) \right] \\
&= -108bTe^{-a/T} l_1 + \frac{(-12l_1 - 12l_1(l_1^2 + l_2^2) + 24l_1^2 - 24l_2^2)}{P(l_1 + il_2, l_1 - il_2)} \\
&= -108bTe^{-a/T} l_1 + \frac{(-12l_1 + 24l_1^2 - 12l_1^3 - 12l_1 l_2^2 - 24l_2^2)}{P(l_1 + il_2, l_1 - il_2)},
\end{aligned}$$

$$\begin{aligned}
\frac{\partial}{\partial x^\mu} \frac{\partial \mathcal{L}}{\partial (\partial_\mu l_1)} &= \frac{\partial}{\partial x^\mu} \frac{\partial}{\partial (\partial_\mu l_1)} \left[ \frac{\sigma}{2} T^2 (\partial_\mu l_1 \partial^\mu l_1 + \partial_\mu l_2 \partial^\mu l_2) - U(l_1, l_2) \right] \\
&= \frac{\partial}{\partial x^\mu} \sigma T^2 \partial^\mu l_1.
\end{aligned}$$

From  $\frac{\partial l_1}{\partial x^\mu} = \partial_\mu l_1$  and assuming that  $T$  does not depend on  $x^\mu$ , we get

$$\frac{\partial}{\partial x^\mu} \frac{\partial \mathcal{L}}{\partial (\partial_\mu l_1)} = \sigma T^2 \partial^\mu \partial_\mu l_1.$$

Thus, for the equation of motion for the real part of the Polyakov loop we get

$$\sigma T^2 \partial_\mu \partial^\mu l_1 + \frac{\partial}{\partial l_1} U(l_1, l_2) = 0. \quad (3.7)$$

The equation of motion for the imaginary part of the Polyakov loop  $l_2$  can be derived in the same way as for  $l_1$

$$\begin{aligned}
\frac{\partial \mathcal{L}}{\partial l_2} &= \frac{\partial}{\partial l_2} \left[ \frac{\sigma}{2} T^2 (\partial_\mu l_1 \partial^\mu l_1 + \partial_\mu l_2 \partial^\mu l_2) - U(l_1, l_2) \right] \\
&= \frac{\partial}{\partial l_2} U(l_1, l_2) \\
&= \frac{\partial}{\partial l_2} \left[ -bT [54e^{-a/T} (l_1^2 + il_2^2) + \ln P(l_1 + il_2, l_1 - il_2)] \right] \\
&= -108bTe^{-a/T} l_2 + \left[ \frac{1}{P(l_1 + il_2, l_1 - il_2)} \frac{\partial}{\partial l_2} P(l_1 + il_2, l_1 - il_2) \right] \\
&= -108bTe^{-a/T} l_2 + \left[ \frac{1}{P(l_1 + il_2, l_1 - il_2)} \frac{\partial}{\partial l_2} (1 - 6(l_1^2 + l_2^2) - 3(l_1^2 + l_2^2)^2 \right. \\
&\quad \left. + 4(2l_1^3 - 6l_1 l_2^2)) \right] \\
&= -108bTe^{-a/T} l_2 + \frac{(-12l_2 - 12(l_1^2 + l_2^2)l_2 - 48l_1 l_2)}{P(l_1 + il_2, l_1 - il_2)} \\
&= -108bTe^{-a/T} l_2 + \frac{(-12l_2 - 12l_1^2 l_2 + 12l_1 l_2^2 - 48l_1 l_2)}{P(l_1 + il_2, l_1 - il_2)}, \\
\frac{\partial}{\partial x^\mu} \frac{\partial \mathcal{L}}{\partial (\partial_\mu l_2)} &= \frac{\partial}{\partial x^\mu} \frac{\partial}{\partial (\partial_\mu l_2)} \left[ \frac{\sigma}{2} T^2 (\partial_\mu l_1 \partial^\mu l_1 + \partial_\mu l_2 \partial^\mu l_2) - U(l_1, l_2) \right] \\
&= \frac{\partial}{\partial x^\mu} \sigma T^2 \partial^\mu l_2.
\end{aligned}$$

From  $\frac{\partial l_2}{\partial x^\mu} = \partial_\mu l_2$  where  $T$  again does not depend on  $x^\mu$ , we get

$$\frac{\partial}{\partial x^\mu} \frac{\partial \mathcal{L}}{\partial (\partial_\mu l_2)} = \sigma T^2 \partial^\mu \partial_\mu l_2.$$

Thus, for the equation of motion for the real part of the Polyakov loop we get

$$\sigma T^2 \partial_\mu \partial^\mu l_2 + \frac{\partial}{\partial l_2} U(l_1, l_2) = 0. \quad (3.8)$$

Equations (3.7) and (3.8), will later be used to simulate the dynamics of the Polyakov loop solved by some numerical method in chapter **IV**. Note that, considering figures 2.1 to 2.3, we can see that  $l_1$  is fit for distinguishing between confined and

deconfined phase similar to  $|\langle L \rangle|$ , whereas  $l_2$  is fit for distinguishing between three types of center domains in the deconfined phase.



# CHAPTER IV

## SIMULATION METHOD

Studying the evolution of the center domains can be done by a *time-dependent Polyakov loop simulation* which numerically solves the equations of motion (3.7) and (3.8) in (3+1)-dimensions. The given space-time lattices are 1) space-time lattice for the real part of the Polyakov loop  $l_1$ , 2) space-time lattice for the imaginary part of the Polyakov loop  $l_2$ . Note again, confined and deconfined state of the system can be distinguished by  $|\langle L \rangle|$ , on the other hand types of the center domains cannot be distinguished by  $|\langle L \rangle|$  but rather  $l_2$ , see section 2.1.

### 4.1 Numerical implementation

Solving equations (3.7) and (3.8) requires some numerical method. In (Cassol-Seewald et al., 2012), a useful method for solving partial differential equations is provided, to apply that method to our problem, we start from writing equations (3.7) and (3.8) into a discrete form

$$\sigma T^2 \left( \frac{\partial^2 l_{n-1}}{\partial t^2} - \vec{\nabla}^2 l_{n-1} \right) + \frac{\partial}{\partial l_{n-1}} U(l_1, l_2) = 0, \quad (4.1)$$

$l_n$  here corresponds to either the real part of the Polyakov loop  $l_1$  or the imaginary part of the Polyakov loop  $l_2$  at time interval  $n$  where time  $t = n\Delta t$  with  $n = 1, 2, 3, \dots$  We

can write the time derivatives as

$$\begin{aligned}\frac{\partial l_{n-1}}{\partial t} &= \dot{l}_{n-1} = \frac{1}{2}(\dot{l}_{n-1/2} + \dot{l}_{n-3/2}), \\ \dot{l}_{n-1/2} &= \frac{1}{\Delta t}(l_n - l_{n-1}), \\ \dot{l}_{n-3/2} &= \frac{1}{\Delta t}(l_{n-1} - l_{n-2}), \\ \frac{\partial^2 l_{n-1}}{\partial t^2} &= \ddot{l}_{n-1} = \frac{1}{\Delta t^2}(\dot{l}_{n-1/2} - \dot{l}_{n-3/2}).\end{aligned}$$

Equation (4.1) becomes

$$\begin{aligned}\sigma T^2 \left( \frac{1}{\Delta t^2}(l_n - 2l_{n-1} + l_{n-2}) - \vec{\nabla}^2 l_{n-1} \right) + \frac{\partial}{\partial l_{n-1}} U(l_1, l_2) &= 0, \\ l_n &= 2l_{n-1} - l_{n-2} + \Delta t^2 \left( \vec{\nabla}^2 l_{n-1} - \frac{1}{\sigma T^2} \frac{\partial}{\partial l_{n-1}} U(l_1, l_2) \right).\end{aligned}\quad (4.2)$$

Consider the Laplacian operator

$$\begin{aligned}\vec{\nabla}^2 l_{ijk}^{n-1} &= \frac{\partial^2 l_{ijk}^{n-1}}{\partial^2 x} + \frac{\partial^2 l_{ijk}^{n-1}}{\partial^2 y} + \frac{\partial^2 l_{ijk}^{n-1}}{\partial^2 z} \\ &= \frac{1}{\Delta x} \left[ \left( \frac{l_{i+1jk}^{n-1} - l_{ijk}^{n-1}}{\Delta x} \right) - \left( \frac{l_{ijk}^{n-1} - l_{i-1jk}^{n-1}}{\Delta x} \right) \right. \\ &\quad \left. + \left( \frac{l_{ij+1k}^{n-1} - l_{ijk}^{n-1}}{\Delta x} \right) - \left( \frac{l_{ijk}^{n-1} - l_{ij-1k}^{n-1}}{\Delta x} \right) \right. \\ &\quad \left. + \left( \frac{l_{ijk+1}^{n-1} - l_{ijk}^{n-1}}{\Delta x} \right) - \left( \frac{l_{ijk}^{n-1} - l_{ijk-1}^{n-1}}{\Delta x} \right) \right] \\ &= \frac{1}{\Delta x^2} [l_{i+1jk}^{n-1} + l_{ij+1k}^{n-1} + l_{ijk+1}^{n-1} - 6l_{ijk}^{n-1} + l_{i-1jk}^{n-1} + l_{ij-1k}^{n-1} + l_{ijk-1}^{n-1}],\end{aligned}$$

where  $i, j$  and  $k$  are positions on the Cartesian grid and  $\Delta x$  is the lattice spacing. We

apply periodic boundary conditions for the spatial coordinates

$$i = \begin{cases} N + i, & \text{if } i < 1. \\ i - N, & \text{if } i > N. \\ i, & \text{otherwise.} \end{cases}\quad (4.3)$$

where  $i$  is a position on the  $x$ -,  $y$ - or  $z$ -axis and  $N$  is the maximum size of the space-time lattice in one dimension. In the equations of motion (4.2), the value of the Polyakov loop at any time  $t$  can be calculated from its previous values at times  $n - 1$  and  $n - 2$ .

## 4.2 Numerical parameters

**Table 4.1** Numerical parameters.

Variable	Meaning	Value
$\Delta t$	time step	0.005 (fm/c)
$\Delta x$	lattice spacing	0.5 (fm)
$N$	size of lattice in one dimension	100

Note that the values of  $\Delta t$  and  $\Delta x$  are determined according to the Courant–Friedrichs–Lewy condition where the ratio of  $\Delta t/\Delta x$  is supposed to be small enough to ensure numerical stability.  $N$  has to be chosen large enough for the lattice to be able to contain several larger domains. However, our choice of these numerical parameters is also based on several test runs.

## 4.3 Initial conditions

At times  $t = 0.005$  fm/c and  $t = 0.01$  fm/c, both real and imaginary part of the Polyakov loop are initialized with Gaussian distributions of mean zero, corresponding to their vacuum expectation value, and standard deviation 0.1. From figure 4.1, we can see small fluctuations of the Polyakov loop correlated over a typical hadron-sized volume of

$1 \text{ fm}^3$ . This corresponds to the initial state in a heavy-ion collision before the creation of the QGP. We can then change the temperature on our lattice to some value above  $T_c$  and follow the evolution of the system in the deconfined phase, where the initial fluctuations can amplify and form center domains.

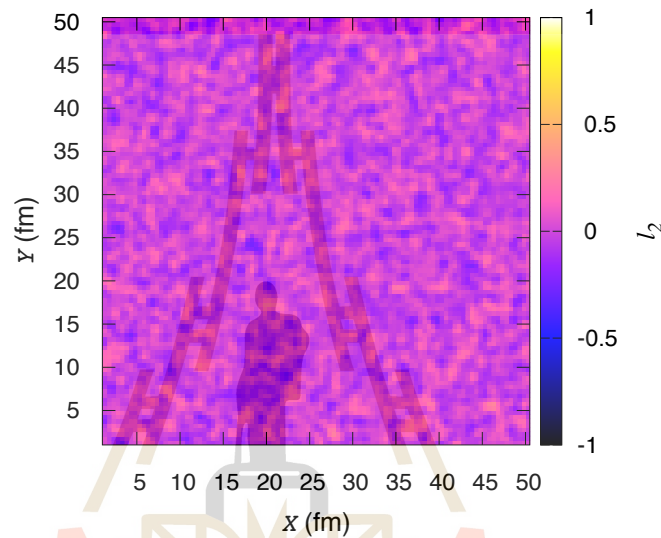


**Figure 4.1** Small fluctuations in Polyakov loop at  $z = 0 \text{ fm}$  and time  $t = 0.005 \text{ fm}/c$ .

#### 4.4 Fixing sigma

According to the equations of motion (3.7) and (3.8), there is one unknown variable called *sigma* ( $\sigma$ ), a coefficient playing the role of a surface tension which influences the domain size, a large value of sigma gives a large domain size, by contrast, a small value of sigma gives a small domain size, see figure 4.2. In order to develop a realistic model, we need to fix the value of sigma. In figure 4.3 from (Borsanyi et al., 2011), some useful information about the domain size as function of  $T$  is provided. The domain size is defined as a physical diameter  $D_{phy}$  which is obtained from fitting the

two-point correlation function  $C(\vec{x} - \vec{y})$  of  $l_2$  to the exponential function

$$C(\vec{x} - \vec{y}) \propto \exp(-|\vec{x} - \vec{y}| / D_{phy}). \quad (4.4)$$

Unfortunately, (Borsanyi et al., 2011) does not give us more data for higher temperatures, so we can only make predictions for these given values and give a rough estimate for sigma as a function of temperature in the regime near  $T_c$ . Thus in this work we consider only the temperatures  $T_1 = 1.05 T_c = 283.5$  MeV,  $T_2 = 1.1 T_c = 297.0$  MeV and  $T_3 = 1.15 T_c = 310.5$  MeV.

We fix the coefficient  $\sigma$  using the following procedure:

1. Fix value of  $T$  according to information in figure 4.3,
2. Heuristically fix value of  $\sigma$ ,
3. Run a simulation,
4. Calculate  $D_{phy}$ ,
5. Compare given  $D_{phy}$  to figure 4.3,
6. If  $D_{phy}$  does not equal its value in figure 4.3, go back to step 2.

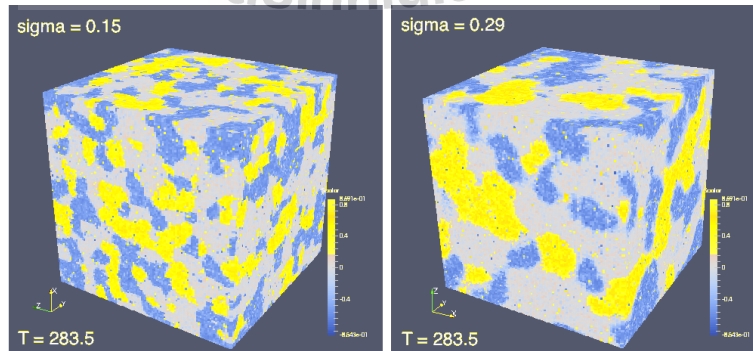


**Figure 4.2** Space-time lattices with a different sigma values.

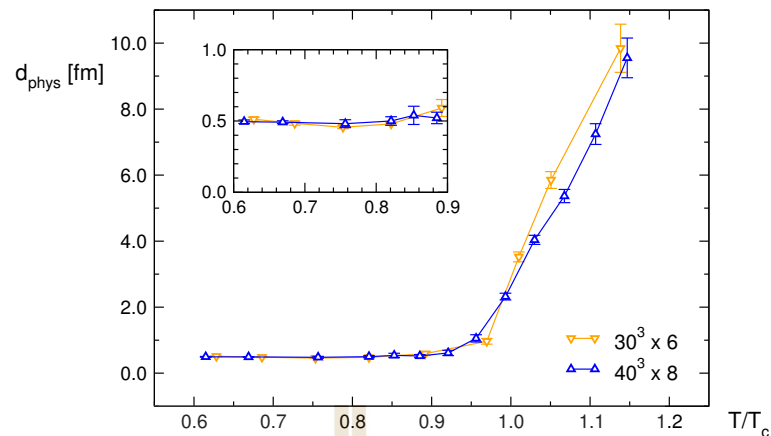


**Figure 4.3** Average diameter of domains for two resolution scales, (Borsanyi et al., 2011).

Fast fixing of sigma can be done by a following *binary search strategy*

**Searching procedure:**

1. Find value of *middle* from list *l*,
2. Compare *target* to *middle*,
3. If *target* less than *middle* then:
  - remove *middle* and its right-hand side values from list *l* then go to 1;
  - else if *target* greater than *middle* then:
    - remove *middle* and its left-hand side values from list *l* then go to 1;
    - else: stop.

where *l* is list of values, *middle* is a value at middle of list *l*, *target* is a value that we want to find.

**Example:**

Problem: find a target value  $target = 8$  in a sorted list  $l = [0, 1, 2, 3, 4, 5, 6, 7, 8, 9, 10]$ .

Define  $middle$  as a value at middle of  $l$ ,  $middle = 5$ . (1<sup>st</sup> procedure)

Is  $target = 8$  equal to  $middle = 5$ ? (2<sup>nd</sup> procedure)

False, then let  $l = [6, 7, 8, 9, 10]$ . (3<sup>rd</sup> procedure)

Define  $middle$  as a value at middle of  $l$ ,  $middle = 8$ . (1<sup>st</sup> procedure)

Is  $target = 8$  equal to  $middle = 8$ ? (2<sup>nd</sup> procedure)

True, stop. (3<sup>rd</sup> procedure)

After finishing the iterative process of fixing sigma, we will obtain a reliable coefficient to study the dynamics of domain formation in the range from  $1 T_c$  to  $1.2 T_c$ .

#### 4.5 Tracking evolution of center domains

Since  $l_1$  distinguishes between confined and deconfined phase,  $l_2$  identifies the type of minimum points in center domains. Both  $l_1$  and  $l_2$  are evolve from confined to deconfined phase. In the deconfined phase, the existence of center domains is expected. This leads to the question how to determine the time when center domains are formed. Our solution proposes to solve this problem by using the *standard deviation (SD)*.

The standard deviation at time  $t$  is defined as

$$SD = \sqrt{\frac{1}{N^3} \sum_{i,j,k} (l_{2ijk} - \bar{l}_2)^2}, \quad (4.5)$$

where  $\bar{l}_2$  is volume-averaged value of  $l_2$ . If SD has reached a stable maximum value as a function of time, we can conclude that the domain formation process is finished. Note that, in our research, the standard deviation is then averaged over 100 events with different initial conditions for each time  $t$  to ensure reliable results.

## CHAPTER V

### RESULTS

#### 5.1 Sigma coefficient

Applying the iterative method introduced in section 4.4, we can obtain a reliable value of sigma. In figure 5.1, we show the result of sigma for temperature  $T_1$  where the dots indicate the two-point correlation function of  $l_2$  and the solid line is the fitted exponential function (5.1) which is evaluated as

$$C(\vec{x} - \vec{y}) \propto \exp(-|\vec{x} - \vec{y}| / 2.55 \text{ fm}). \quad (5.1)$$

The exponential function for temperature  $T_2$  is

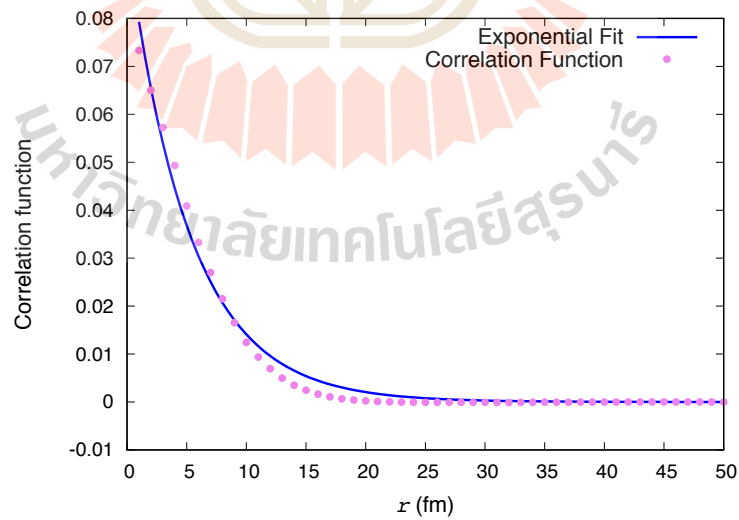


**Figure 5.1** Exponential fit of the correlation function for  $T = 283.5$  MeV.

$$C(\vec{x} - \vec{y}) \propto \exp(-|\vec{x} - \vec{y}| / 3.75 \text{ fm}), \quad (5.2)$$

see figure 5.2 for the corresponding graph. For  $T_3$  we obtain

$$C(\vec{x} - \vec{y}) \propto \exp(-|\vec{x} - \vec{y}| / 4.75 \text{ fm}). \quad (5.3)$$

The fitted correlation function of sigma for temperature  $T_3$ , is shown in figure 5.3. Finally, we put all results of sigma to one graph in figure 5.4 and show sigma as function of  $T$  and fit it to a third order polynomial:

$$\sigma(T) = (1.37 \times 10^{-5}(T - T_c)^3) / \text{MeV}^3 + 0.10. \quad (5.4)$$

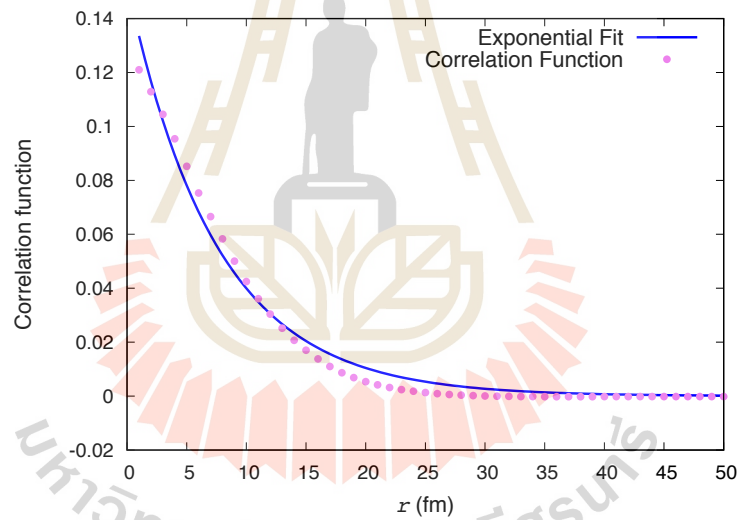


**Figure 5.2** Exponential fit of the correlation function for  $T = 297.0 \text{ MeV}$ .

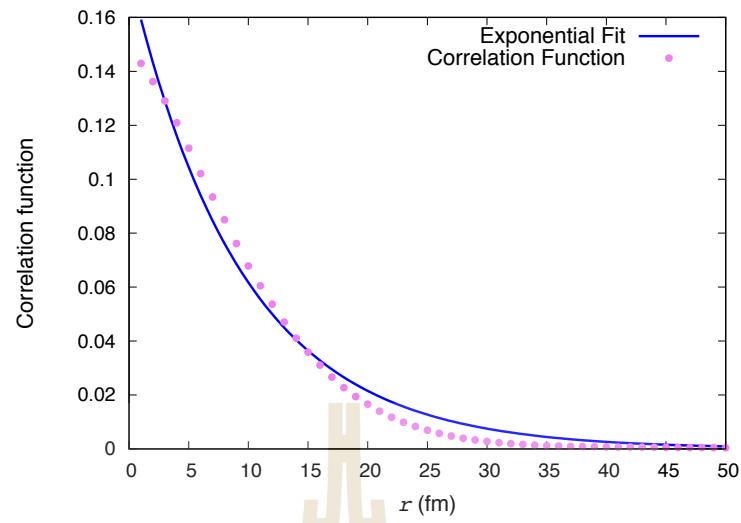


**Figure 5.3** Exponential fit of the correlation function for  $T = 310.5$  MeV.

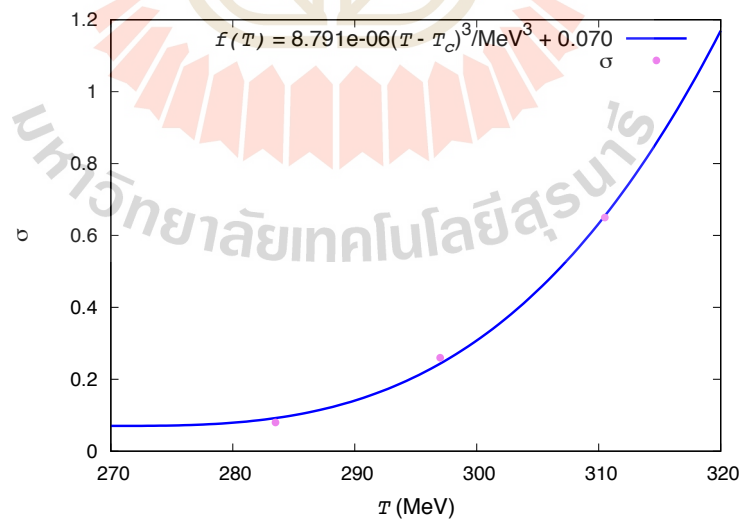


**Figure 5.4** Sigma as a function of temperature.

## 5.2 Formation of center domains

We study the time evolution of center domains via the average value of the standard deviation of  $l_2$ . Note again, in our simulation, there are only three distinct temperatures that we will consider according to the information in figure 5.4, that are  $T_1 = 1.05 T_c = 283.5 \text{ MeV}$ ,  $T_2 = 1.1 T_c = 297.0 \text{ MeV}$  and  $T_3 = 1.15 T_c = 310.5 \text{ MeV}$ . From the simulation, we obtain three graphs of the standard deviation as a function of time, see figures 5.5, 5.6 and 5.7.

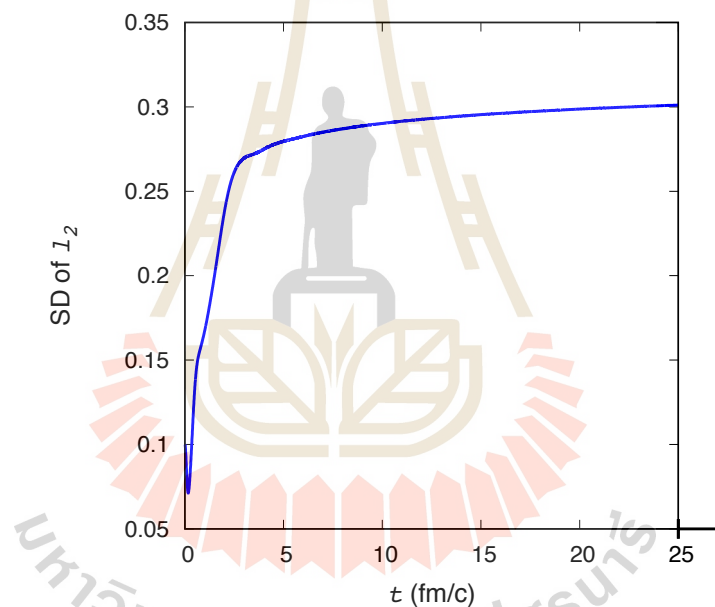


**Figure 5.5** Evolution of standard deviation from time 0 - 25 fm/c with  $T_1$ .

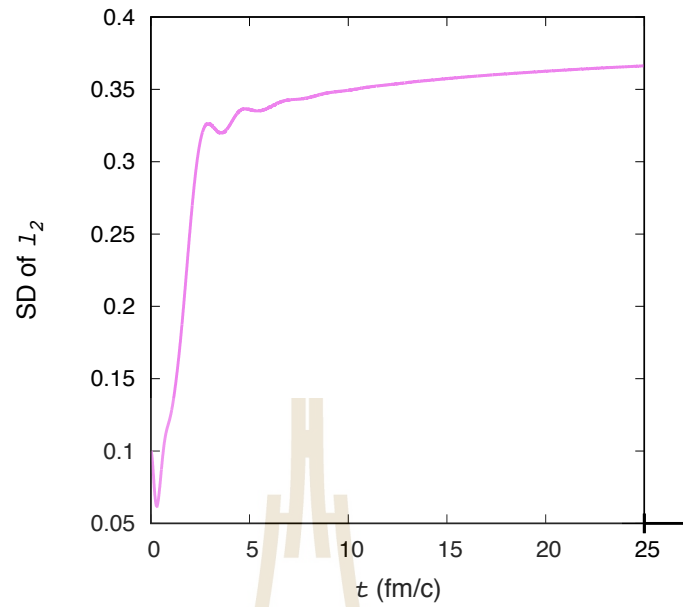


**Figure 5.6** Evolution of standard deviation from time 0 - 25 fm/c with  $T_2$ .

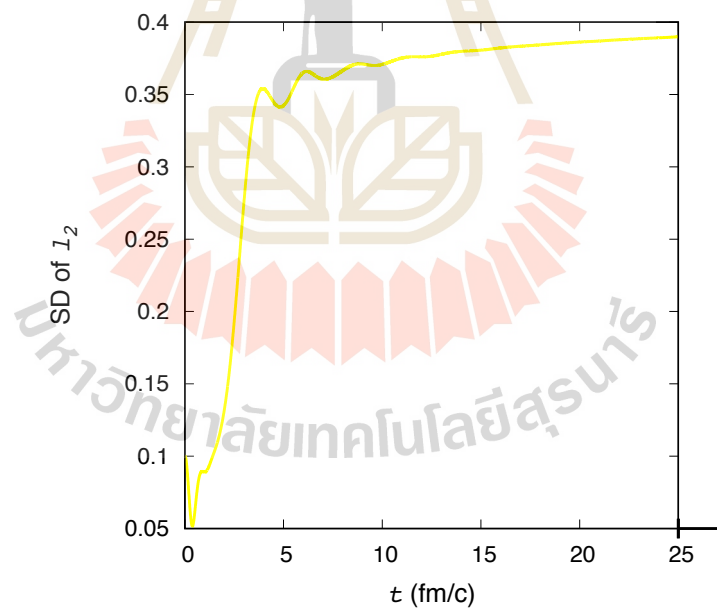


**Figure 5.7** Evolution of standard deviation from time 0 - 25 fm/c with  $T_3$ .

Finally, we put those three graphs into a comparing graph

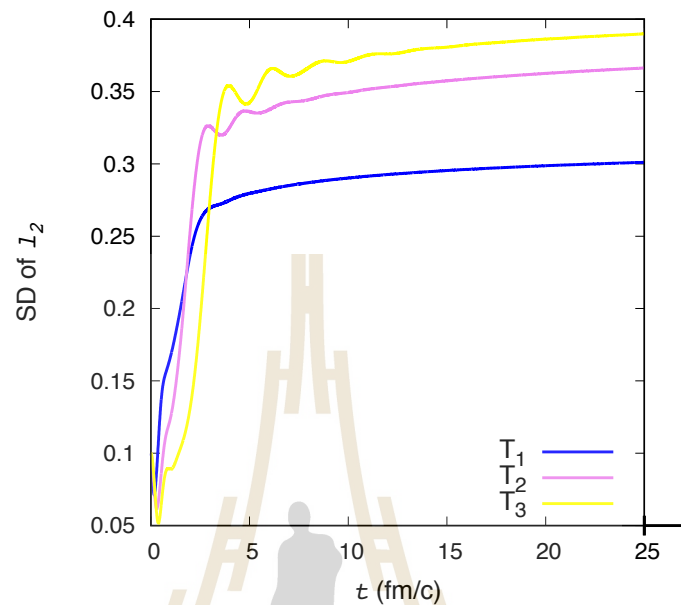


**Figure 5.8** Evolution of standard deviation from time 0 - 25 fm/c with  $T_1$ ,  $T_2$  and  $T_3$ .

We can clearly identify the center domains by plotting  $l_2$  as a function of  $x$  and  $y$  for a constant  $z$  which is shown in figures 5.9 to 5.11. From the plots in figures 5.9 to 5.11, we can follow the formation of the center domains over time starting from small fluctuations at the initial state to the final state where we can clearly see the pattern of the center domains at time  $t = 25$  fm/c. When the center domains are fully developed, the border lines between them are more sharp, the expansion of domains has stopped, and only very small fluctuations occur. From figures 5.9 to 5.11, we can also see that size of center domains is influenced by sigma, a higher sigma value of sigma results in a larger size of center domains.

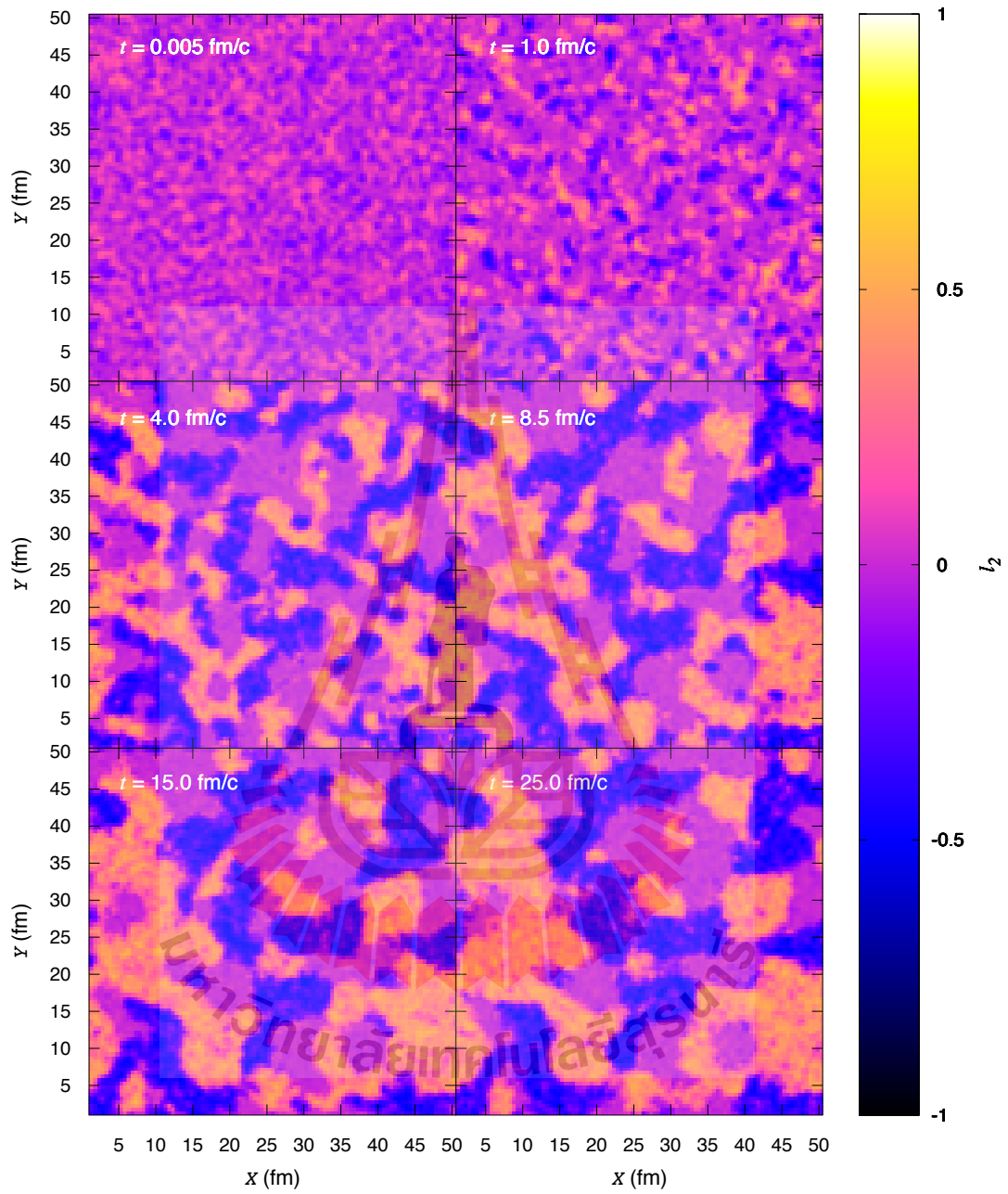


**Figure 5.9** Plan plot of  $l_2$  from time 0 - 25 fm/c with  $T_1$ .

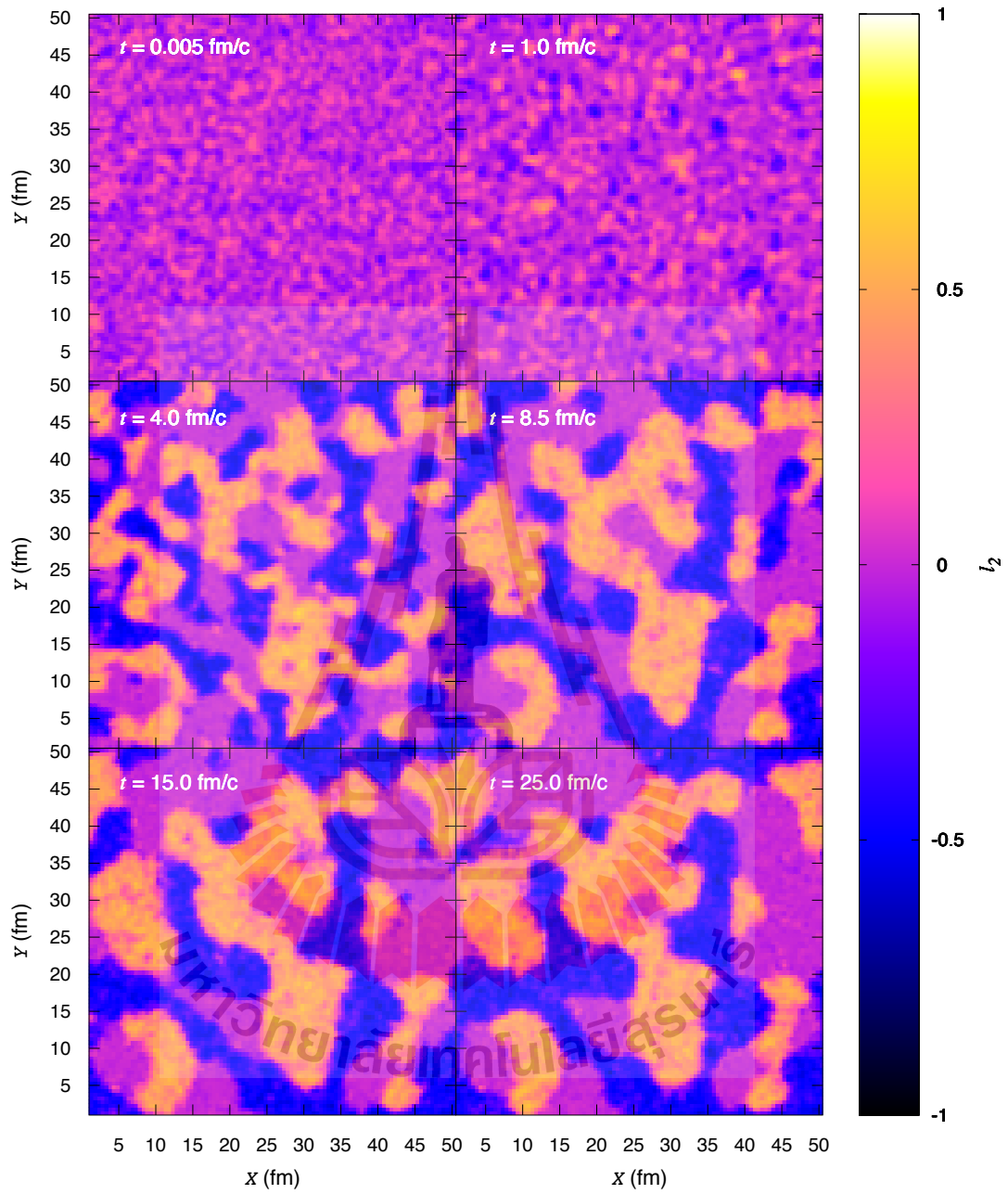


**Figure 5.10** Plan plot of  $l_2$  from time 0 - 25 fm/c with  $T_2$ .

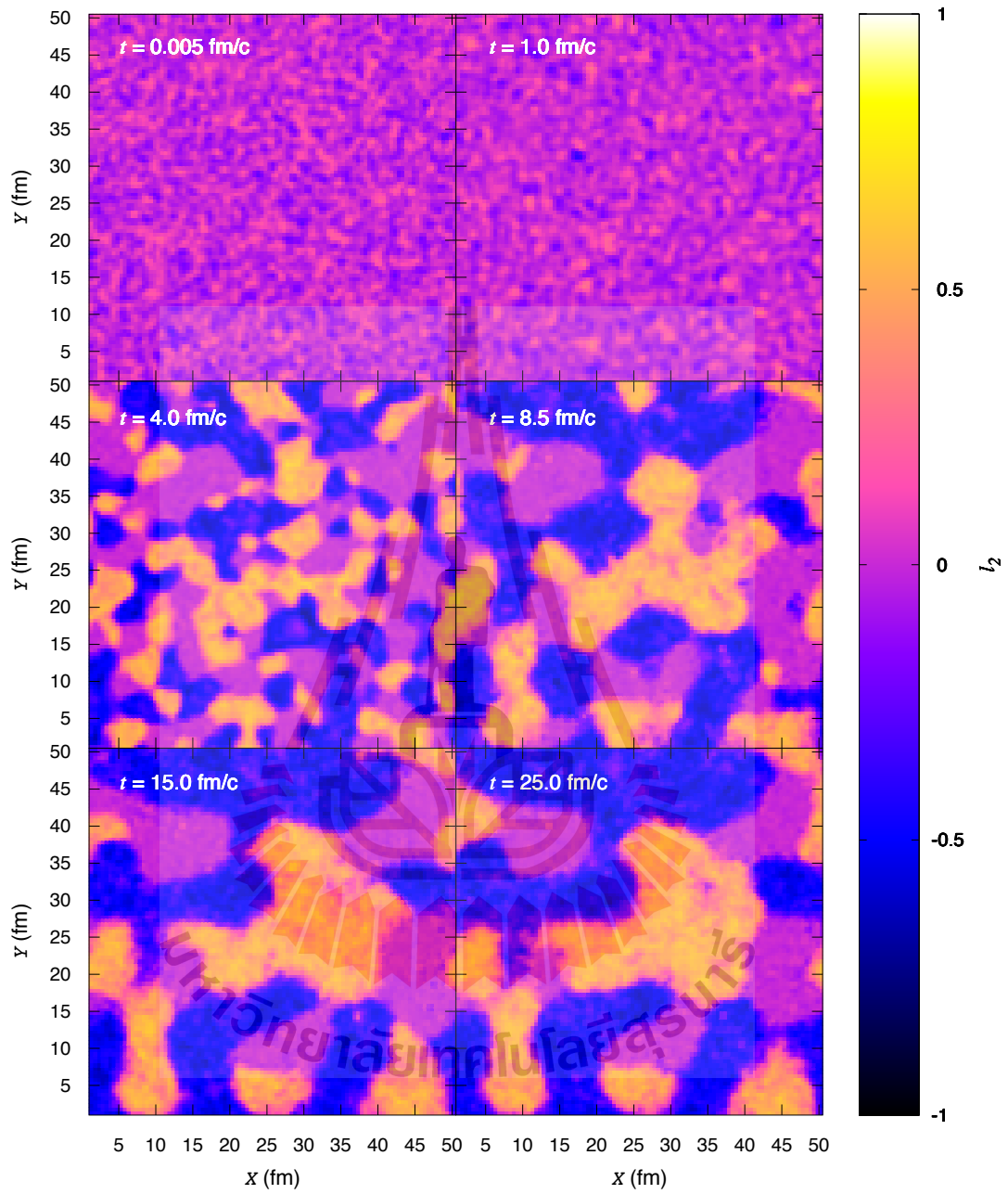


**Figure 5.11** Plan plot of  $l_2$  from time 0 - 25 fm/c with  $T_3$ .

### 5.3 Decay of center domains

We now study the decay of center domains via the average value of the standard deviation of  $l_2$ . Here, the standard deviation is defined again as in equation (4.5). After finishing the formation of center domains at  $t = 25$  fm/c, we suddenly decrease all temperatures to a new value  $T_1 = T_2 = T_3 = 200$  MeV. With this temperature below  $T_c$ , the center domains will start to decay. Investigation of decay of center domains here is started from  $t = 26$  to 50 fm/c. Thus, from the simulation we obtain three graphs of standard deviation versus time, see figures 5.12, 5.13 and 5.14.

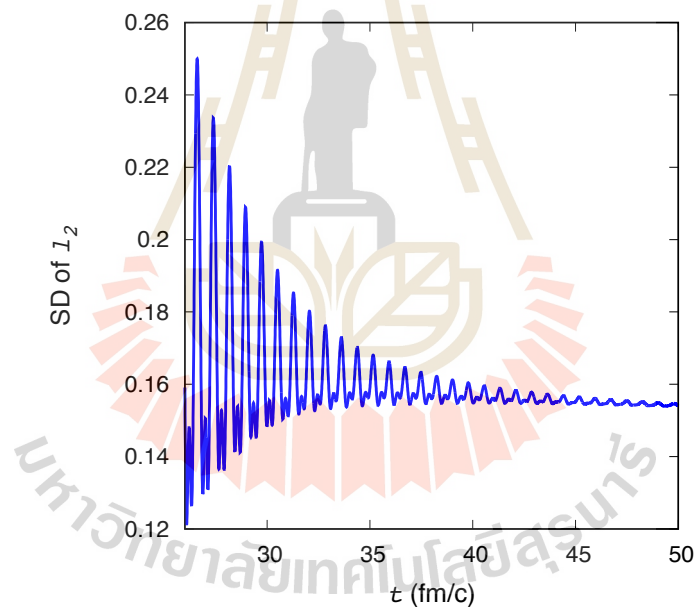


**Figure 5.12** Evolution of standard deviation from time 26 - 50 fm/c with  $T_1$ .

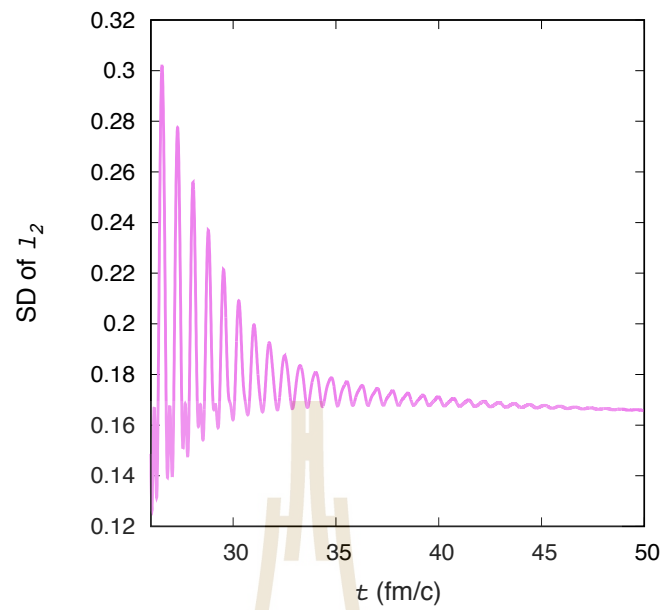


**Figure 5.13** Evolution of standard deviation from time 26 - 50 fm/c with  $T_2$ .

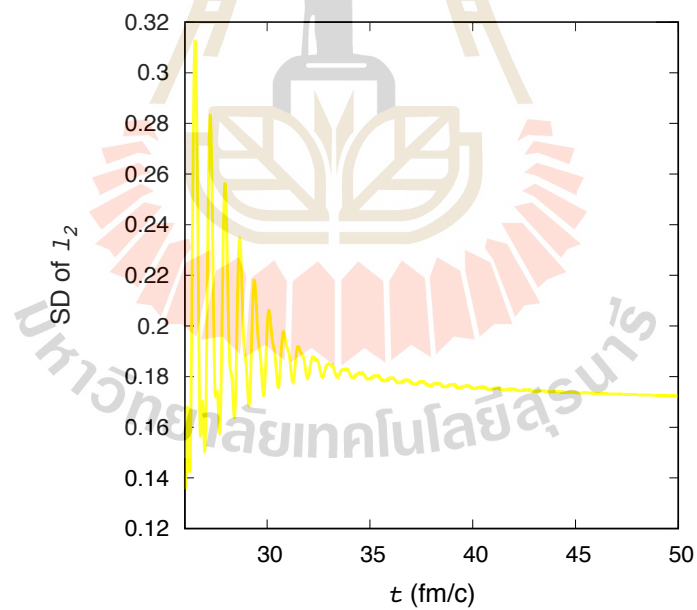


**Figure 5.14** Evolution of standard deviation from time 26 - 50 fm/c with  $T_3$ .

Finally, we put those three graphs into a comparing graph

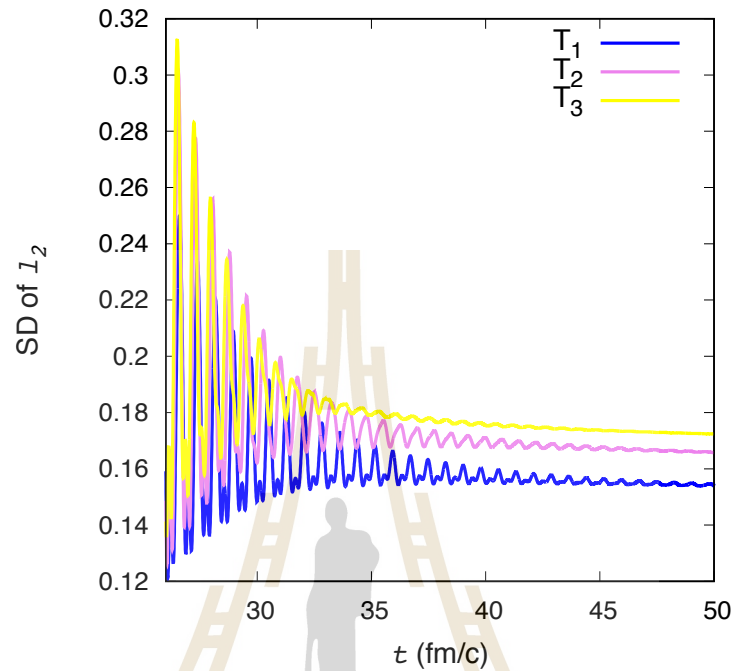


**Figure 5.15** Evolution of standard deviation from time 26 - 50 fm/c with  $T_1$ ,  $T_2$  and  $T_3$

We can clearly identify center domains by plotting  $l_2$  as a function of  $x$  and  $y$  for constant  $z$  which is shown in figures 5.16 to 5.21. To investigate the decay of center domains, we focus on times when upper and lower peaks in standard deviations occur. Considering times at upper peaks, the center domains slowly decay to some small fluctuation state which looks similar to an initial state of our simulation. These final states have some unique values of the standard deviation depending on temperature. Focusing on lower peaks, center domains decay extremely fast to a fluctuation state which has a value of standard deviation lower than the final state. However, these standard deviation will be increased from peak to peak until the final state is reached.

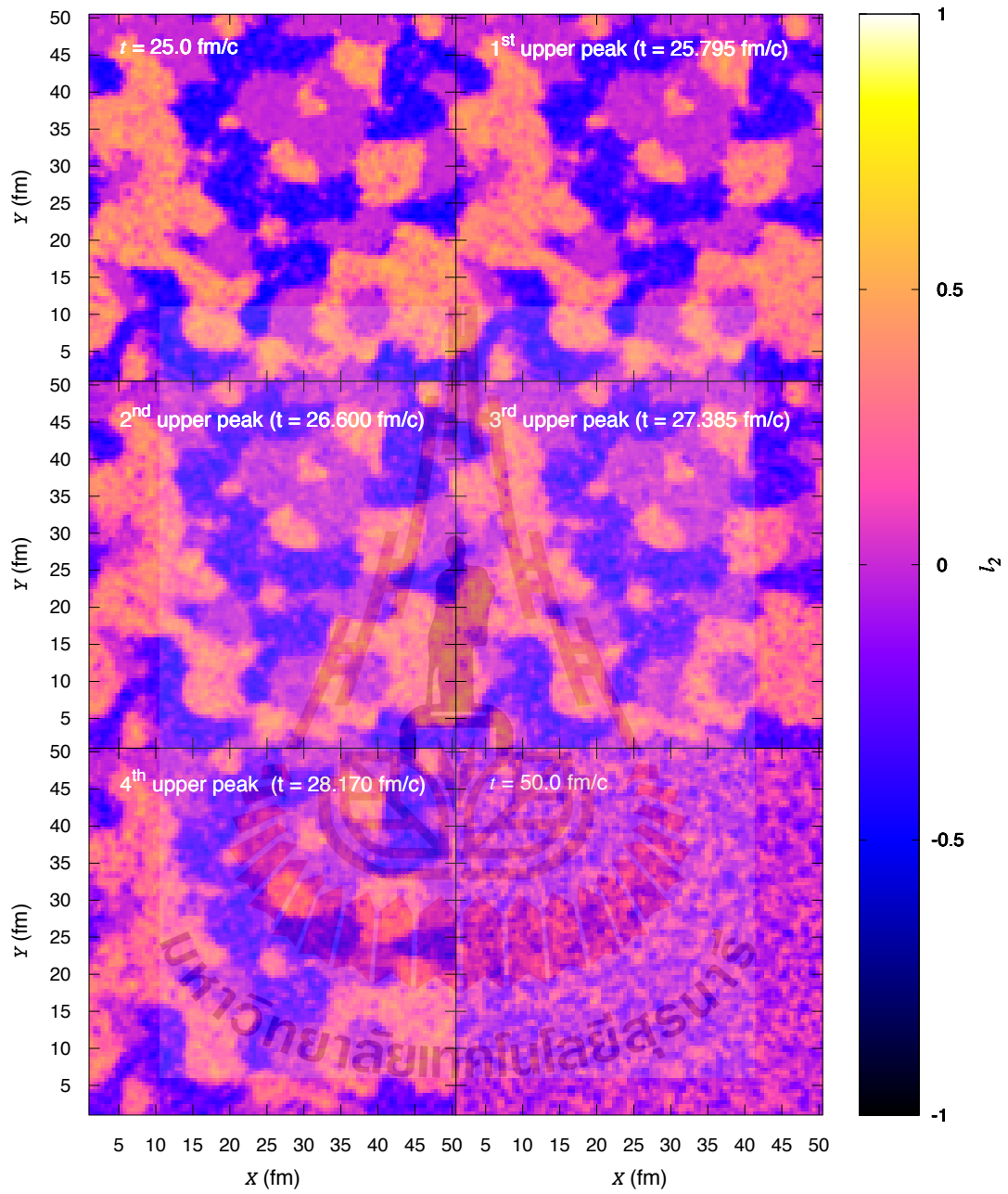


**Figure 5.16** Plan plot of  $l_2$  from time 26 - 50 fm/c with  $T_1$ .

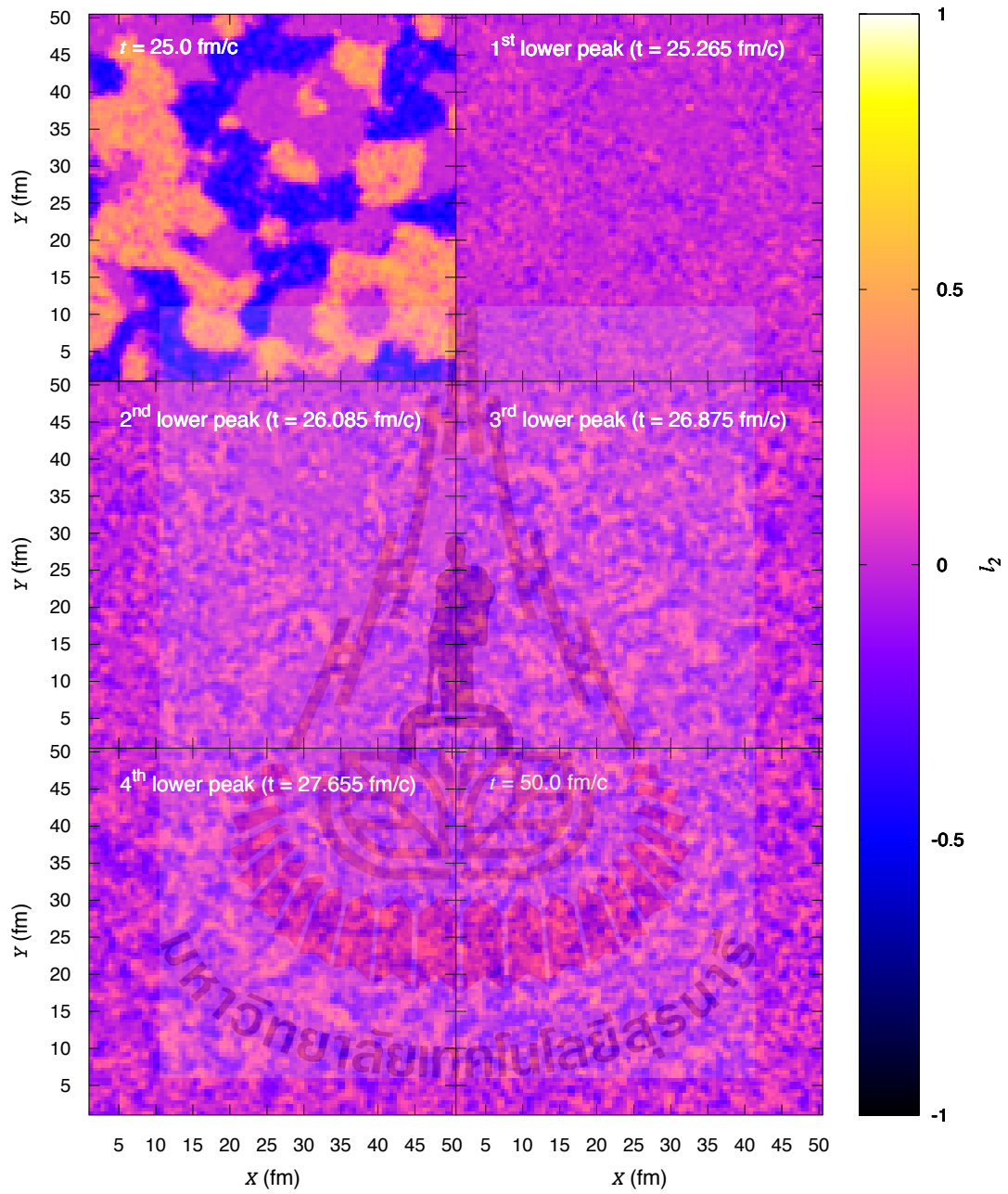


**Figure 5.17** Plan plot of  $l_2$  from time 26 - 50 fm/c with  $T_1$ .

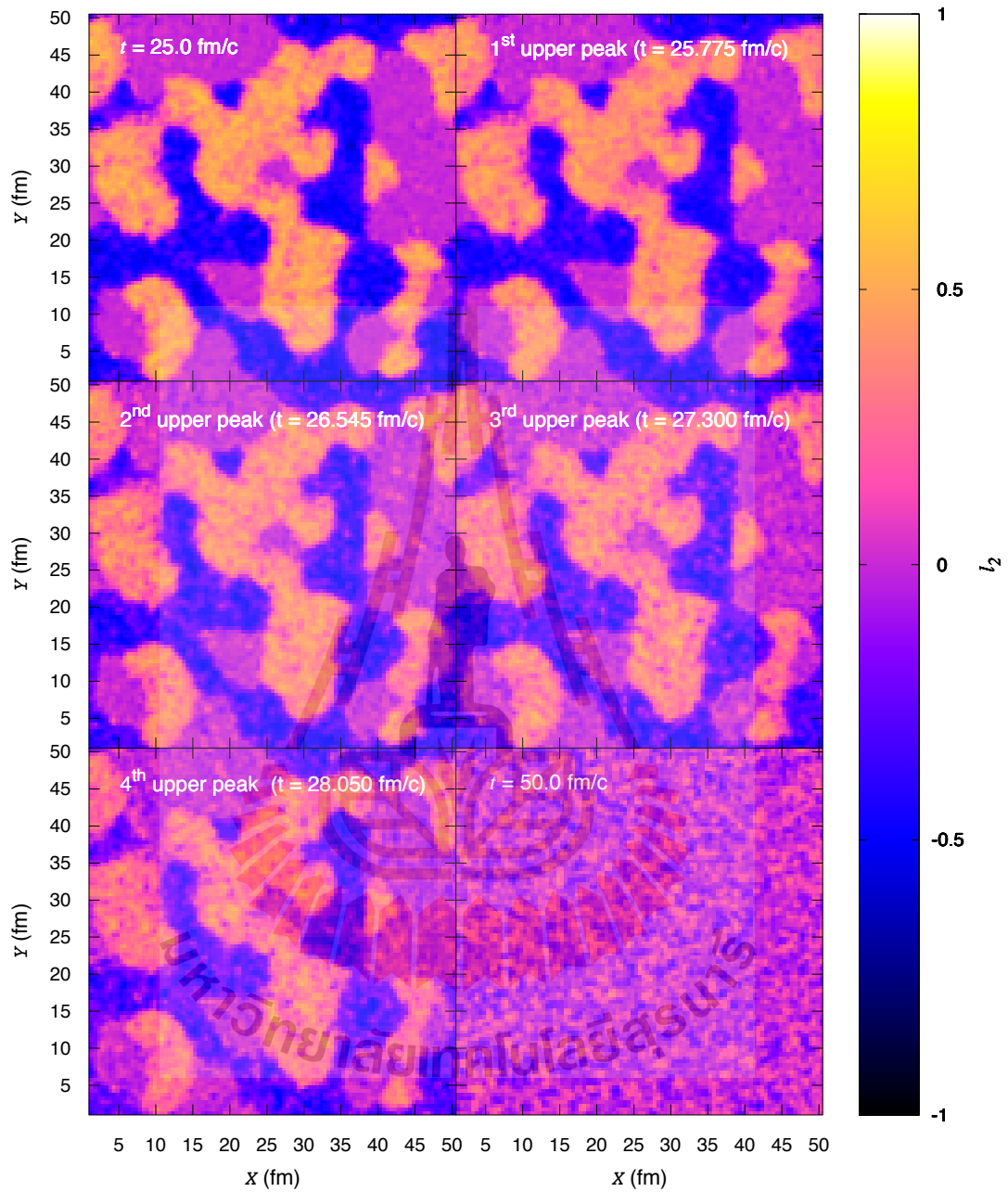


**Figure 5.18** Plan plot of  $l_2$  from time 26 - 50 fm/c with  $T_2$ .

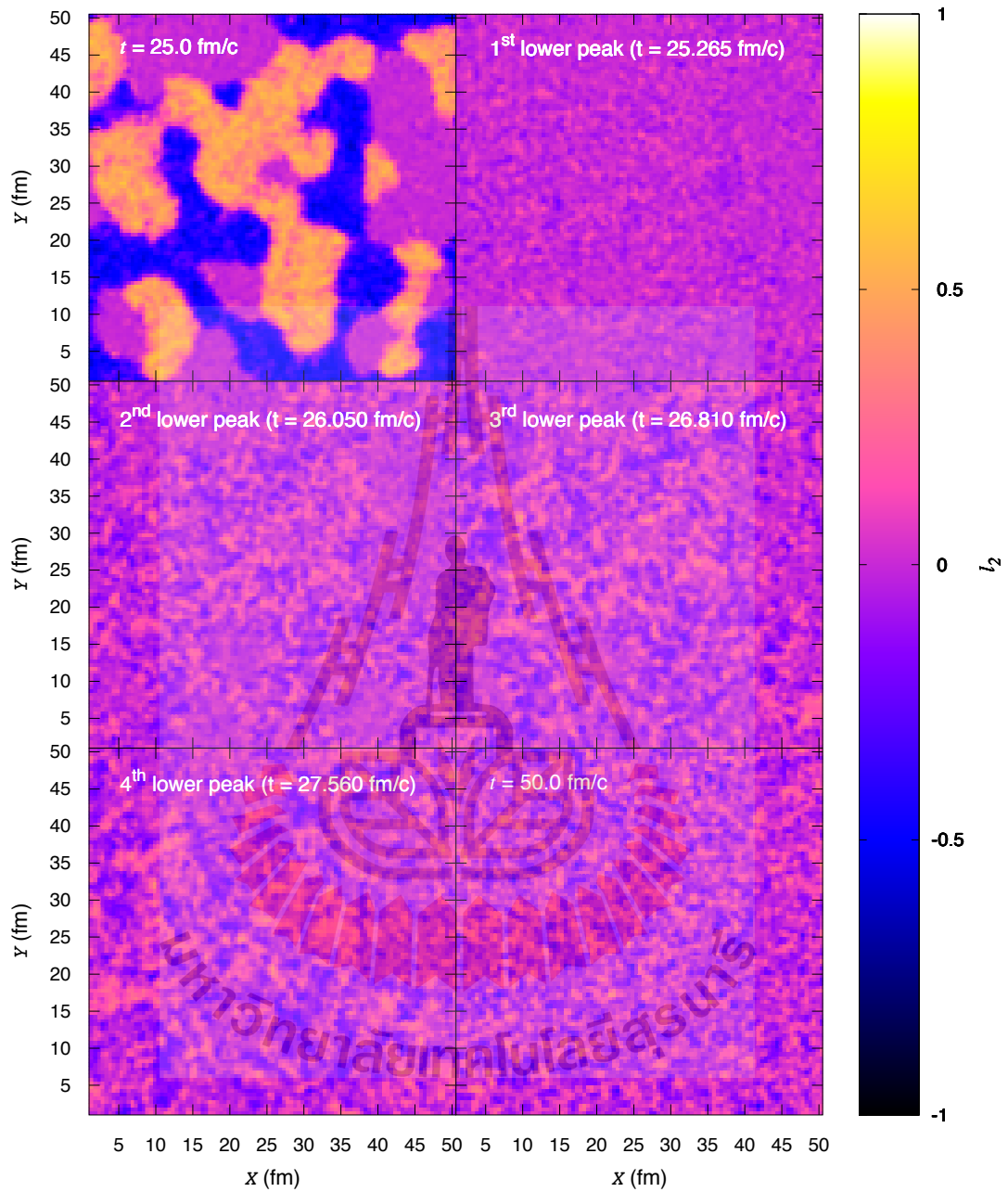


**Figure 5.19** Plan plot of  $l_2$  from time 26 - 50 fm/c with  $T_2$ .

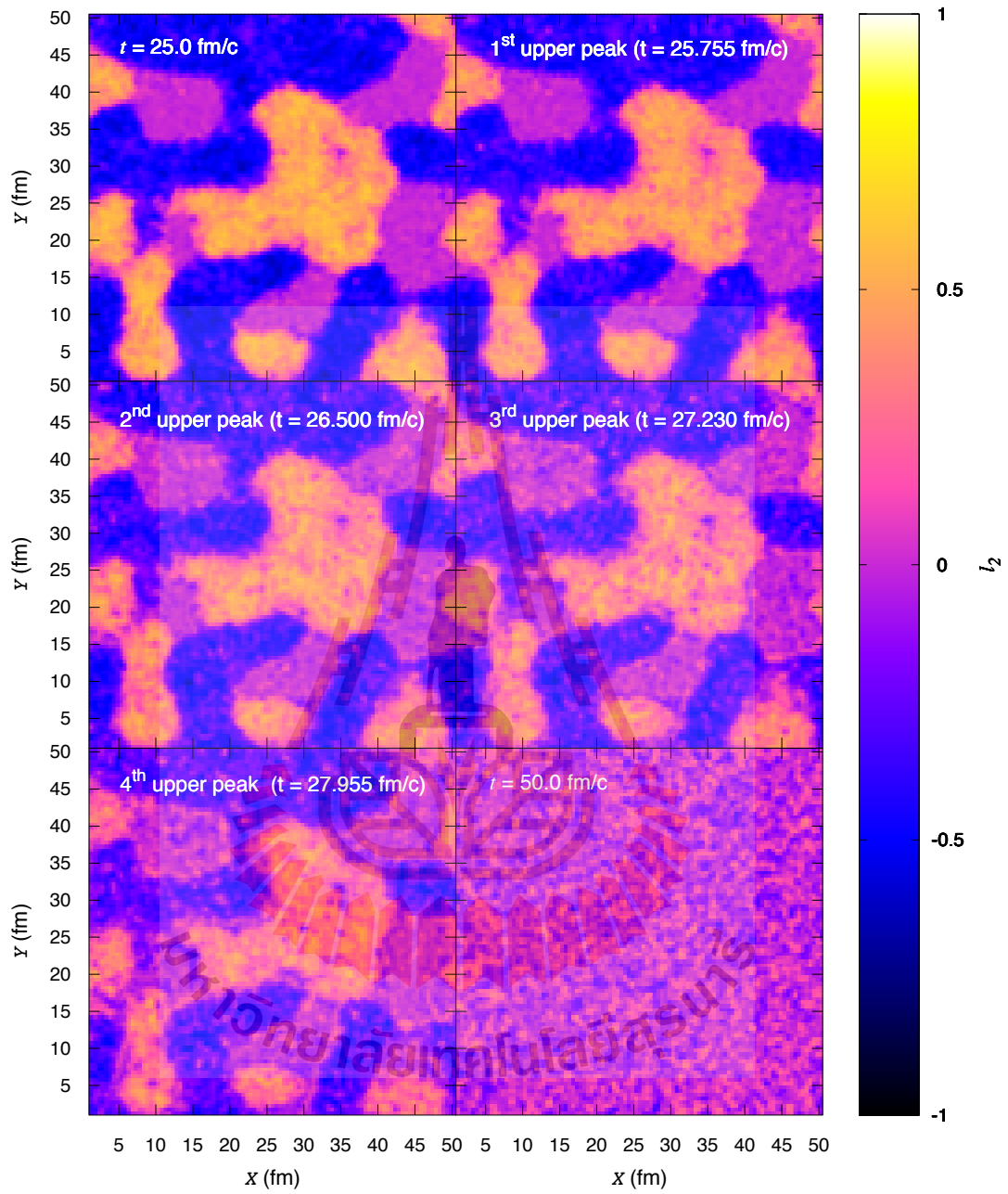


**Figure 5.20** Plan plot of  $l_2$  from time 26 - 50 fm/c with  $T_3$ .

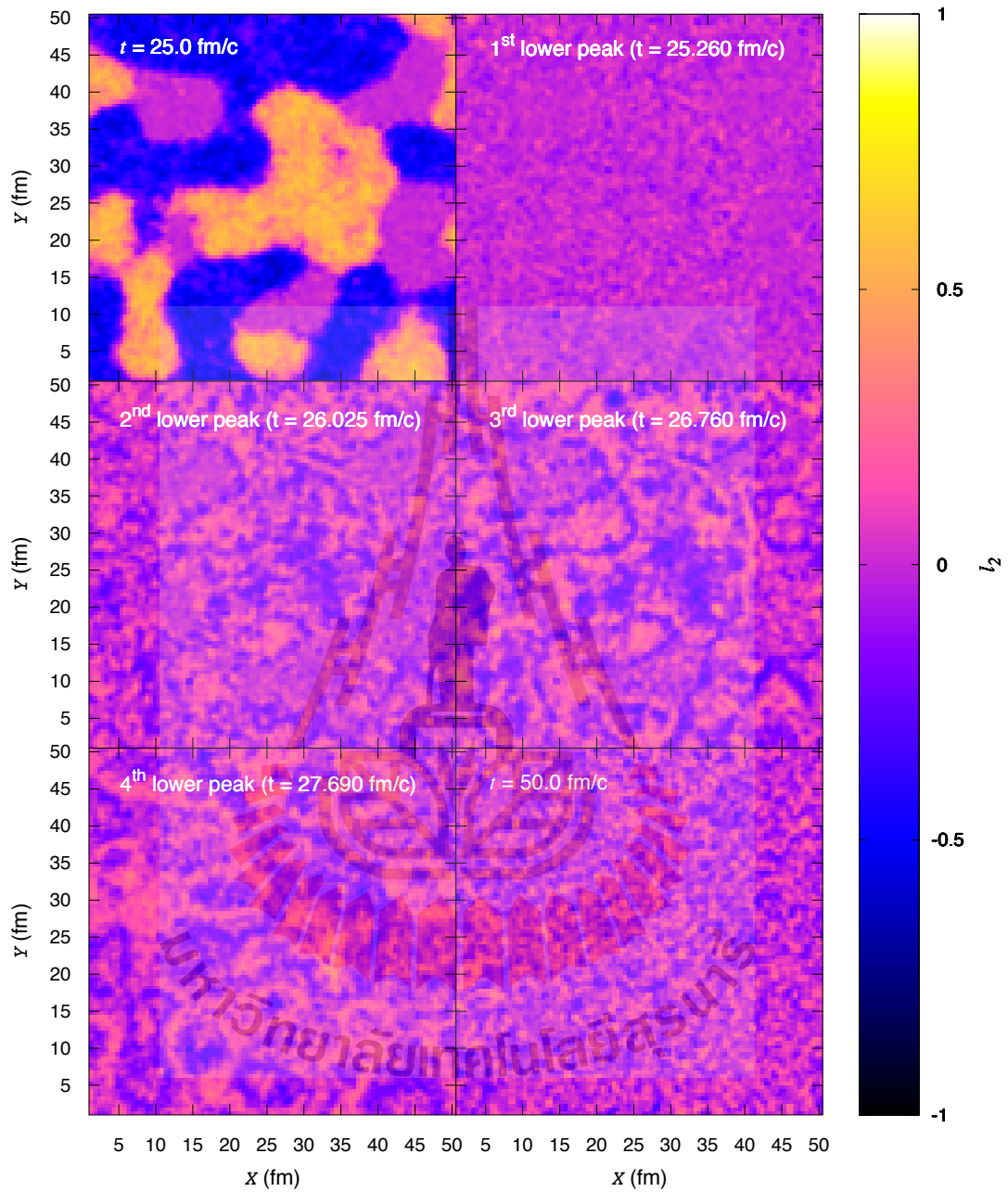


**Figure 5.21** Plan plot of  $l_2$  from time 26 - 50 fm/c with  $T_3$ .

# CHAPTER VI

## CONCLUSIONS AND DICUSSIONS

In pure gauge theory, the Polyakov loop has the ability to distinguish between confined and deconfined phase. By constructing an effective Lagrangian from the Polyakov loop potential and a phenomenological kinetic term we can obtain equations of motion (3.7) and (3.8). Studying the evolution of the center domains in QGP can be done by a time-dependent Polyakov loop simulation which solves the equations of motion for the Polyakov loop value in (3+1) dimensions. In (Borsanyi et al., 2011), the domain size is shown to be dependent on temperature, furthermore, in our work, the domains size is also influenced by the surface tension ( $\sigma$ ) which is a coefficient in the equations of motion (3.7) and (3.8). At high temperature or sigma, the domain size is big while at low temperature or sigma, the domain size is small, see figures 4.3 and 5.4. From our simulation, the result shows that, during the formation, small fluctuations around zero in the initial state evolve into domain structures with three different types of domains according to local breakdown of  $Z_3$  symmetry. From our simulation, the estimated formation time of center domains is about 3 – 7 fm/c, see figure 5.8, significantly smaller than the estimated QGP lifetime in heavy-ion collision from (Bass and Dumitru, 2000) which is about 13 fm/c, see figure 6.1. The model that used in (Bass and Dumitru, 2000) is Hydro + UrQMD model. Here, open symbols show distributions for a purely hydrodynamical calculation, solid symbols show the

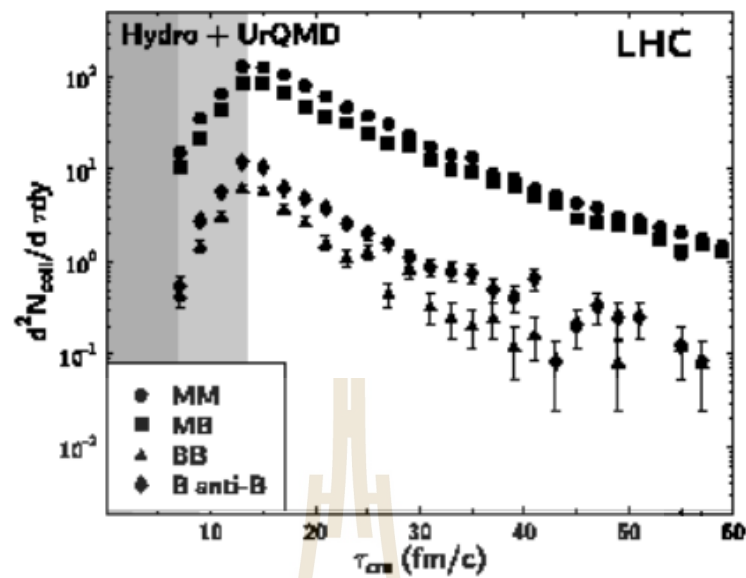
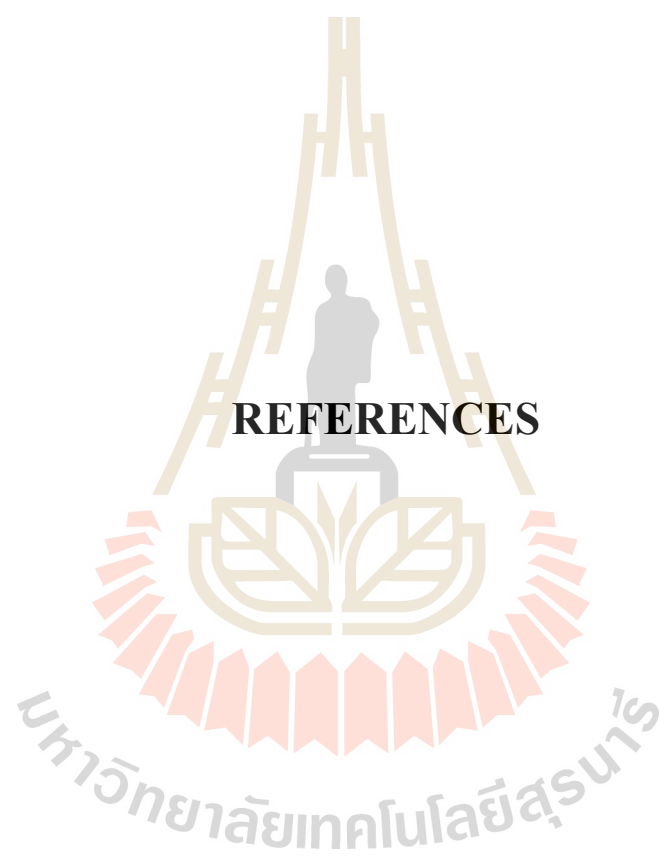


**Figure 6.1** Heavy-ion collision rates at LHC energy.

full calculation with hadronic rescattering. The given formation time is short enough to make center domains possible and necessary to consider in a QGP state. We can see fluctuations in the deviation during the decay of center domains, which takes about  $7 - 20$  fm/c before returning to a state with small fluctuations at temperatures below  $T_c$ .



**REFERENCES**

## REFERENCES

- Adams, J., Aggarwal, M., Ahammed, Z., Amonett, J., Anderson, B., Arkhipkin, D., Averichev, G., Badyal, S., Bai, Y., Balewski, J., Barannikova, O., Barnby, L., Baudot, J., Bekele, S., Belaga, V., Bellingeri-Laurikainen, A., Bellwied, R., Berger, J., Bezverkhny, B., Bharadwaj, S., et al. (2005). Experimental and theoretical challenges in the search for the quark–gluon plasma: The star collaboration’s critical assessment of the evidence from rhic collisions. **Nuclear Physics A**. 757(1-2): 102-183. First Three Years of Operation of RHIC.
- Adcox, K., Adler, S., Afanasiev, S., Aidala, C., Ajitanand, N., Akiba, Y., Al-Jamel, A., Alexander, J., Amirikas, R., Aoki, K., Aphecetche, L., Arai, Y., Armendariz, R., Aronson, S., Averbeck, R., Awes, T., Azmoun, R., Babintsev, V., Baldisseri, A., Barish, K., et al. (2005). Formation of dense partonic matter in relativistic nucleus–nucleus collisions at rhic: Experimental evaluation by the phenix collaboration. **Nuclear Physics A**. 757(1-2): 184-283. First Three Years of Operation of RHIC.
- Aoki, Y., Endrodi, G., Fodor, Z., Katz, S., and Szabo, K. (2006). The order of the quantum chromodynamics transition predicted by the standard model of particle physics. **Nature**. 443: 675-678.
- Arsene, I., Bearden, I., Beavis, D., Besliu, C., Budick, B., Bøggild, H., Chasman, C., Christensen, C., Christiansen, P., Cibor, J., Debye, R., Enger, E., Gaardhøje, J., Germinario, M., Hansen, O., Holm, A., Holme, A., Hagel, K., Ito, H., Jakobsen, E.,

- et al. (2005). Quark–gluon plasma and color glass condensate at rhic the perspective from the brahms experiment. **Nuclear Physics A**. 757(1-2): 1-27. First Three Years of Operation of RHIC.
- Asakawa, M., Bass, S., and Müller, B. (2013). Center domains and their phenomenological consequences. **Physical Review Letter**. 110(20): 202301.
- Back, B., Baker, M., Ballintijn, M., Barton, D., Becker, B., Betts, R., Bickley, A., Bindel, R., Budzanowski, A., Busza, W., Carroll, A., Chai, Z., Decowski, M., García, E., Gburek, T., George, N., Gulbrandsen, K., Gushue, S., Halliwell, C., Hamblen, J., et al. (2005). The phobos perspective on discoveries at rhic. **Nuclear Physics A**. 757(1-2): 28-101. First Three Years of Operation of RHIC.
- Bass, S. and Dumitru, A. (2000). Dynamics of hot bulk qcd matter: From the quark-gluon plasma to hadronic freeze-out. **Physical Review C**. 61: 064909.
- Borsanyi, S., Danzer, J., Fodor, Z., Gattlinger, C., and Schmidt, A. (2011). Coherent center domains from local polyakov loops. **Journal of Physics: Conference Series**. 312: 012005.
- Boyd, G., Engels, J., Karsch, F., Laermann, E., Legeland, C., Lutgemeier, M., and Petersson, B. (1996). Thermodynamics of su(3) lattice gauge theory. **Nuclear Physics**. B469: 419-444.
- Cassol-Seewald, N., Farias, R., Fraga, E., Krein, G., and Ramos, R. (2012). Langevin simulation of scalar fields: Additive and multiplicative noises and lattice renormalization. **Physica A: Statistical Mechanics and its Applications**. 391(16): 4088-4099.

- Danzer, J., Gatttringer, C., Borsanyi, S., and Fodor, Z. (2010). Center clusters and their percolation properties in lattice qcd. **Proceedings of Science**. LATTICE2010: 176.
- Dumitru, A. and Pisarski, R. (2001). Event-by-event fluctuations from decay of a polyakov loop condensate. **Physics Letters**. B504: 282-290.
- Fraga, E., Krein, G., and Mizher, A. (2007). Langevin dynamics of the pure  $su(2)$  deconfining transition. **Physical Review**. D76: 034501.
- Fukushima, K. (2004). Chiral effective model with the polyakov loop. **Physics Letters B**. 591(3-4): 277-284.
- Gyulassy, M. and McLerran, L. (2005). New forms of qcd matter discovered at rhic. **Nuclear Physics A**. 750(1): 30-63. Quark–Gluon Plasma. New Discoveries at RHIC: Case for the Strongly Interacting Quark–Gluon Plasma. Contributions from the RBRC Workshop held May 14–15, 2004.
- Herbst, T., Pawłowski, J., and Schaefer, B. (2011). The phase structure of the polyakov-quark-meson model beyond mean field. **Physics Letters**. B696: 58-67.
- Herold, C., Nahrgang, M., Mishustin, I., and Bleicher, M. (2013). Chiral fluid dynamics with explicit propagation of the polyakov loop. **Physical Review**. C87: 014907.
- Müller, B. and Nagle, J. L. (2006). Results from the relativistic heavy ion collider. **Annual Review of Nuclear and Particle Science**. 56(1): 93-135.
- Roessner, S., Ratti, C., and Weise, W. (2007). Polyakov loop, diquarks and the two-flavour phase diagram. **Physics Review**. D75: 034007.
- Scavenius, O., Mocsy, A., Mishustin, I., and Rischke, D. (2001). Chiral phase transition

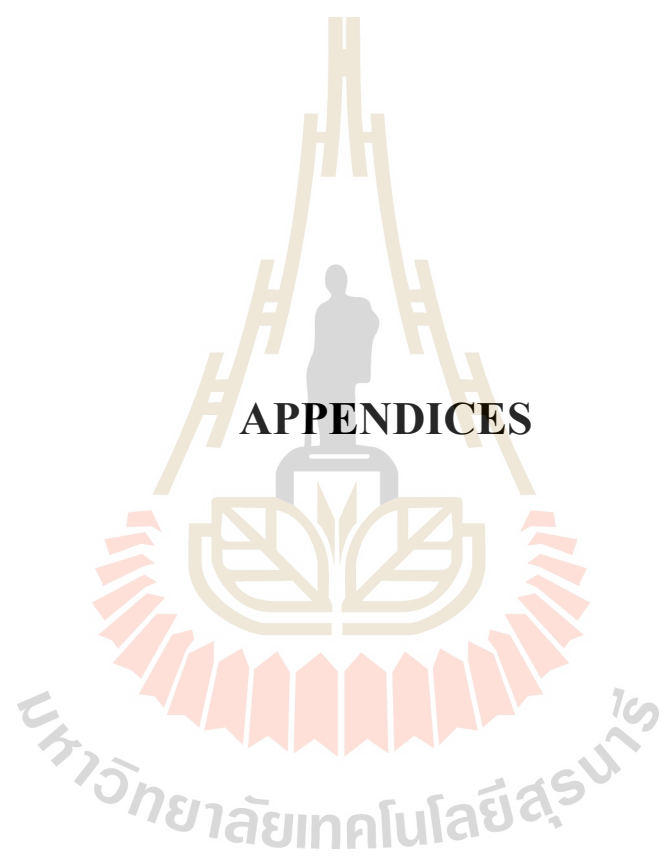
within effective models with constituent quarks. **Physical Review**. C64: 045202.

Schaefer, B., Pawłowski, J., and Wambach, J. (2007). The phase structure of the polyakov-quark-meson model. **Physical Review**. D76: 074023.

Schaefer, B. and Wambach, J. (2005). The phase diagram of the quark meson model.

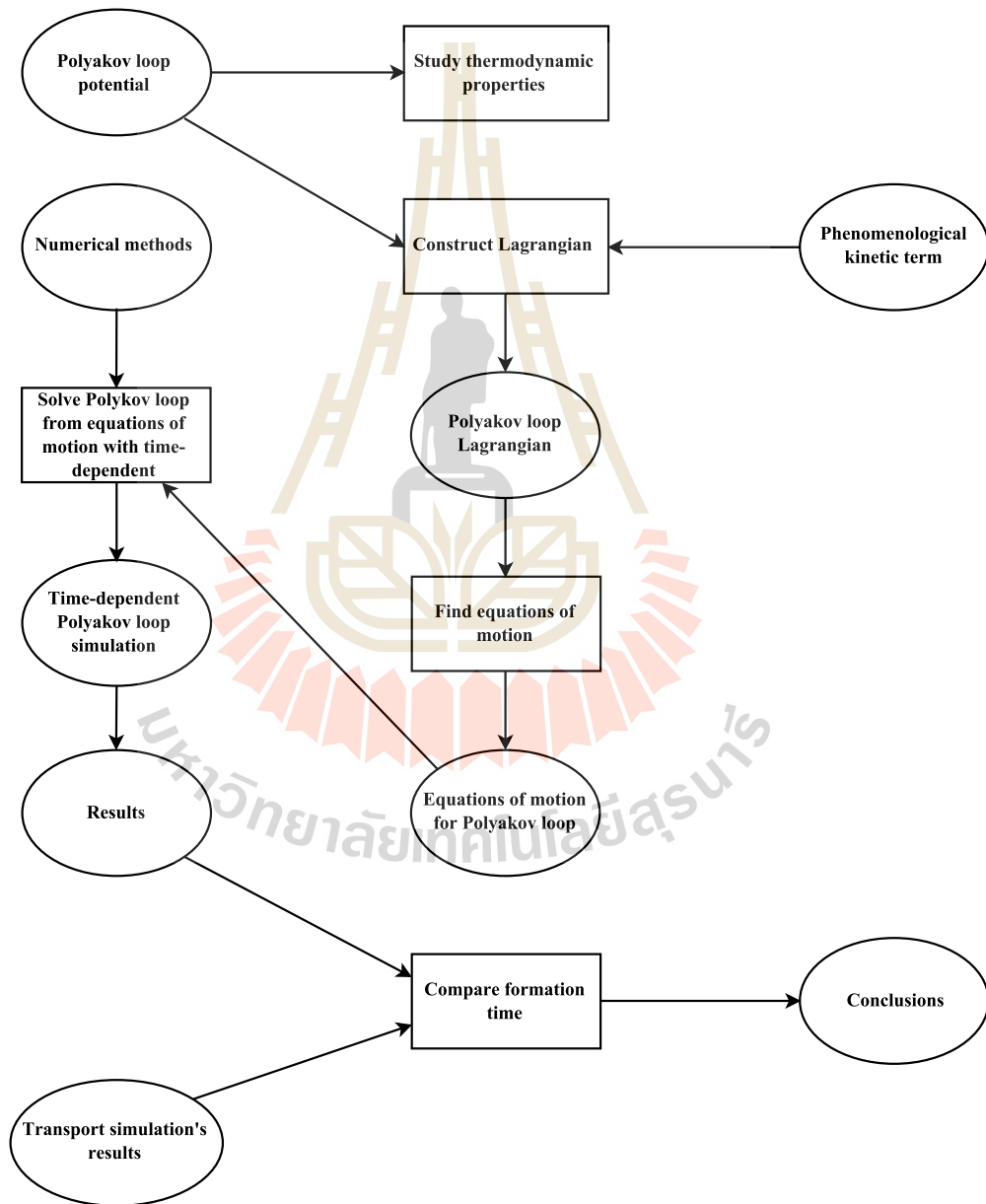
**Nuclear Physics**. A757: 479-492.





# APPENDIX A

## RESEARCH WORKFLOW



## APPENDIX B

### NATURAL UNITS

In natural units  $\hbar = c = k_B = 1$ , we have

$$\hbar = \frac{h}{2\pi} = 6.5821 \times 10^{-25} \text{ GeV} \cdot \text{s} = 1, \quad (0.1)$$

and

$$c = 2.9979 \times 10^8 \text{ m} \cdot \text{s}^{-1} = 1, \quad (0.2)$$

where  $h$  is the Planck constant,  $\hbar$  is the reduced Planck constant,  $c$  is the speed of light,  $k_B$  is the Boltzmann constant. From equations 0.1 and 0.2, we obtain a useful relation

$$\hbar c = 1 = (6.5821 \times 10^{-22} \text{ MeV} \cdot \text{s})(2.9979 \times 10^{23} \text{ fm} \cdot \text{s}^{-1}) = 197.3 \text{ MeV} \cdot \text{fm} \quad (0.3)$$

where 1 fm (femtometer or fermi) =  $1 \times 10^{-15}$  m. In high energy physics, energy and mass are frequently measured in a unit of GeV (giga electronvolt), meanwhile length and time are measured in a  $\text{GeV}^{-1}$  or fm. Note that to make a difference between units of length and time, we can write unit of time as fm/c. Due to the relation in equation 0.3, we can easily convert between  $\text{GeV}^{-1}$  and fm. In high energy physics, electromagnetic unit can be measured either in Lorentz–Heaviside units or Gaussian units, see table B.1.

**Table B.1** Natural units in particle physics.

	<b>Unit</b>	<b>Metric value</b>
<b>Length</b>	1 eV <sup>-1</sup>	$1.97 \times 10^{-7}$ m
<b>Time</b>	1 eV <sup>-1</sup>	$6.58 \times 10^{-16}$ s
<b>Mass</b>	1 eV	$1.78 \times 10^{-36}$ kg
<b>Temperature</b>	1 eV	$1.16 \times 10^4$ K
<b>Electric charge</b> <b>(L-H unit)</b>	1 unit of electric charge	$5.29 \times 10^{-19}$ C
<b>Electric charge</b> <b>(Gaussian unit)</b>	1 unit of electric charge	$1.88 \times 10^{-18}$ C

# APPENDIX C

## CODE IMPLEMENTATIONS

Code: Global variables

```
1 module global_vars
2   use, intrinsic :: iso_fortran_env
3   implicit none
4
5   ! variables for Polyakov loop potential
6   real, parameter, public :: a = 664.0 ! [MeV]
7   real, parameter, public :: b = 0.0075e9 ! [MeV^3]
8   real, parameter, public :: hc = 197.3 ! [MeV*fm]
9
10  ! sigma and temperatures
11  real, public :: Temp = 283.5 ! [MeV]
12  real, public :: sigma = 0.08 ! []
13  !-----
14  ! real, public :: Temp = 297 ! [MeV]
15  ! real, public :: sigma = 0.3 ! []
16  !-----
17  ! real, public :: Temp = 310.5 ! [MeV]
18  ! real, public :: sigma = 0.7 ! []
19
20  ! variables for time-dependent Polyakov loop simulation
21  integer, parameter, public :: t_size = 10000 ! [] number of time step
22  integer, parameter, public :: lattice_size = 101 ! [] size of lattice
23  real, parameter, public :: delta_t = 0.005 ! [fm] time interval
24  real, parameter, public :: delta_lattice = 0.5 ! [fm]
25  integer, parameter, public :: x_size = lattice_size ! [] size of x
26  integer, parameter, public :: y_size = lattice_size ! [] size of y
```

## Code (Cont.): Global variables

```

27  integer , parameter , public :: z_size = lattice_size ! [] size of z
28
29  ! constants representing time at 1st, 2nd and 3rd time step
30  integer , parameter , public :: t_at_3 = 3 ! [] constant
31  integer , parameter , public :: t_at_2 = 2 ! [] constant
32  integer , parameter , public :: t_at_1 = 1 ! [] constant
33
34  ! declare array l1 which contains real part Polyakov loop values
35  ! and array l2 contains imaginary part Polyakov loop values
36  real , dimension ( : , : , : ) , allocatable , public :: l1 , l2
37
38  ! array of standard deviations
39  real , dimension ( t_size ) , public :: deviation
40
41  ! output array of correlation function
42  real , dimension ( t_size , int ( lattice_size - 1 ) / 2 ) , public :: r_list
43
44  ! dummy variables for handling index shifting
45  integer , public :: x_plus_1 , y_plus_1 , z_plus_1
46  integer , public :: x_min_1 , y_min_1 , z_min_1
47
48  end module global_vars

```

## Code: Differentiating Potential Function

```

1  module misc_func
2    use global_vars
3    implicit none
4
5    contains
6    ! periodic boundary conditions
7    integer function period_bound_conds(n)
8      implicit none

```

## Code (Cont.): Differentiating potential function

```

9      integer , intent (in) :: n
10
11     if(n < 1) then
12         period_bound_conds = lattice_size + n
13     else if(n > lattice_size ) then
14         period_bound_conds = n - lattice_size
15     else
16         period_bound_conds = n
17     end if
18
19     return
20 end function period_bound_conds
21
22 ! apply PBCs
23 subroutine apply_period_bound_conds(z, y, x)
24     implicit none
25     integer , intent (in) :: z, y, x
26
27     x_min_1 = period_bound_conds(x - 1)
28     y_min_1 = period_bound_conds(y - 1)
29     z_min_1 = period_bound_conds(z - 1)
30     x_plus_1 = period_bound_conds(x + 1)
31     y_plus_1 = period_bound_conds(y + 1)
32     z_plus_1 = period_bound_conds(z + 1)
33
34 end subroutine apply_period_bound_conds
35
36 ! function for finding standard deviation
37 real function find_deviation (1)
38     implicit none
39     real , dimension(z_size, y_size, x_size), intent (in) :: 1
40     integer :: z, y, x
41     real :: l_avg

```

## Code (Cont.): Differentiating potential function

```

42  real :: sum_val
43
44  l_avg = 0.0
45  sum_val = 0.0
46
47  do z = 1, z_size
48      do y = 1, y_size
49          do x = 1, x_size
50              l_avg = l_avg + l(z, y, x)
51          end do
52      end do
53  end do
54
55  l_avg = l_avg / (real(z_size*y_size*x_size))
56
57  do z = 1, z_size
58      do y = 1, y_size
59          do x = 1, x_size
60              sum_val = sum_val + (l(z, y, x) - l_avg)**2
61          end do
62      end do
63  end do
64
65  find_deviation = sqrt(sum_val/real((z_size*y_size*x_size)))
66
67  return
68  end function find_deviation
69
70  end module misc_func

```

Code: Differentiating Potential Function

```

1  module diff_U
2      use global_vars
3      implicit none
4
5      contains
6      ! function for differentiating ln(P) by l1 or l2
7      real function diff_ln_P_func(diff_by, l1, l2)
8          implicit none
9          character(len=2), intent(in) :: diff_by
10         real, intent(in) :: l1, l2
11         real :: P, diff_P, diff_ln_P
12
13         P = (1.0 - 6.0*(l1**2 + l2**2) &
14             - 3.0*(l1**2 + l2**2)**2 &
15             + 4.0*(2.0*l1**3 - 6.0*l1*l2**2))
16
17         diff_ln_P = 1.0/P
18
19         if(diff_by .eq. "l1") then
20             diff_P = (-12.0*l1 - 12.0*(l1**2 + l2**2)*l1 &
21                 + 24.0*l1**2 - 24.0*l2**2)
22         else ! or else if(diff_by .eq. "l2") then
23             diff_P = (-12.0*l2 - 12.0*(l1**2 + l2**2)*l2 - 48.0*l1*l2)
24         end if
25
26         diff_ln_P_func = diff_ln_P*diff_P
27
28         return
29     end function diff_ln_P_func
30
31     ! function for differentiating potential by l1 or l2
32     real function diff_U_func(diff_by, 1, l1, l2)
33         implicit none
34         character(len=2), intent(in) :: diff_by
35         real, intent(in) :: 1, l1, l2
36

```

## Code (Cont.): Differentiating potential function

```

37     diff_U_func = &
38         -b*Temp*(2.0*54.0*exp(-a/Temp)*1 & ! [MeV^3][MeV]
39         + diff_ln_P_func (diff_by , l1 , l2)) & ! [MeV^4]
40         /hc**3                               ! [MeV^3*fm^3]
41
42     return
43 end function diff_U_func
44
45 end module diff_U

```

## Code: Finding Polyakov loop

```

1  module solve_partial_diff
2  use global_vars
3  use misc_func
4  use diff_U
5  implicit none
6
7  contains
8  ! function for solving Laplace function
9  real function laplace_1(l, t, z, y, x)
10     implicit none
11     real , dimension(t_at_3, z_size, y_size, x_size), intent(in) :: l
12     integer , intent(in) :: t, z, y, x
13
14     call apply_period_bound_conds(z, y, x)
15
16     ! operate laplace operator on l
17     laplace_1 = ( &
18         l(t, z, y, x_plus_1) &
19         + l(t, z, y_plus_1, x) &
20         + l(t, z_plus_1, y, x) &
21         - 6.0*l(t, z, y, x) &

```

## Code (Cont.): Finding Polyakov loop

```

22         + l(t, z, y, x_min_1) &
23         + l(t, z, y_min_1, x) &
24         + l(t, z_min_1, y, x) &
25     )/ delta_lattice **2 ! [1/fm^2]
26
27     return
28 end function laplace_1
29
30 ! function for solving diff equation to find Polyakov loop value
31 real function find_l(diff_by, l, t, z, y, x)
32     implicit none
33     character (len=2), intent (in) :: diff_by
34     real, dimension(t_at_3, z_size, y_size, x_size), intent (in) :: l
35     integer, intent (in) :: t, z, y, x
36
37     find_l = ( &
38         2.0*l(t-1, z, y, x) - l(t-2, z, y, x) &
39         + laplace_1(l, t-1, z, y, x) & ! [1/fm^2]
40         * delta_t**2 & ! [fm^2]
41     ) &
42     - ( &
43         diff_U_func(diff_by, l(t-1, z, y, x), & ! [MeV/fm^3]
44         l1(t-1, z, y, x), &
45         l2(t-1, z, y, x)) &
46         *hc & ! [MeV*fm]
47         * delta_t**2 & ! [fm^2]
48     )/(sigma*270.0**2) ! [MeV^2]
49
50     return
51 end function find_l
52
53 end module solve_partial_diff

```

Code: Two-point correlation function

```

1  module two_point_corr
2      use global_vars
3      use misc_func
4      implicit none
5      integer , parameter :: num_round = 1000
6      integer :: center_x, center_y, center_z
7      integer :: start_z, start_y, start_x
8
9      contains
10     ! function for generating arbitrary center points .
11     subroutine rand_center (t)
12         implicit none
13         integer , intent (in) :: t
14         real :: rand_z, rand_y, rand_x
15         integer , dimension(12) :: date_time
16         integer , dimension(12) :: seed
17
18         call date_and_time(values=date_time)
19         call random_seed
20         seed = date_time(6) * date_time(7) + date_time(8)
21         call random_seed(put = seed)
22
23         call random_number(rand_z)
24         center_z = int ( ceiling (rand_z* lattice_size ))
25         call random_number(rand_y)
26         center_y = int ( ceiling (rand_y* lattice_size ))
27         call random_number(rand_x)
28         center_x = int ( ceiling (rand_x* lattice_size ))
29
30         return
31     end subroutine rand_center
32
33     ! function for finding output of correlation function
34     function find_r(t)
35         implicit none

```

## Code (Cont.): Two-point correlation function

```

36 integer , intent (in) :: t
37 integer :: x, y, z, x_index, y_index, z_index
38 integer :: start_x , start_y , start_z
39 integer :: end_x, end_y, end_z
40 integer :: r, i, j, k, round_loop
41 integer :: count_num
42 real , dimension(num_round, int( lattice_size - 1)/2) :: r_list
43 real , dimension(int( lattice_size - 1)/2) :: find_r
44
45
46 do round_loop = 1, num_round
47   call rand_center(t)
48   do r = 1, ( lattice_size - 1)/2
49
50     count_num = 0
51     r_list (round_loop, r) = 0
52
53     start_z = center_z - r
54     start_y = center_y - r
55     start_x = center_x - r
56     end_z = center_z + r
57     end_y = center_y + r
58     end_x = center_x + r
59
60     do z = start_z , end_z
61       do y = start_y , end_y
62         do x = start_x , end_x
63
64           if((x - center_x)**2 + (y - center_y)**2 + &
65             (z - center_z)**2 >= (r - 0.5)**2 .and. &
66             (x - center_x)**2 + (y - center_y)**2 + &
67             (z - center_z)**2 < (r + 0.5)**2) then
68

```

## Code (Cont.): Two-point correlation function

```

69         z_index = period_bound_conds(z)
70         y_index = period_bound_conds(y)
71         x_index = period_bound_conds(x)
72
73         r_list (round_loop, r) = r_list (round_loop, r) +&
74         (l2(t, center_z, center_y, center_x) &
75         *l2(t, z_index, y_index, x_index))
76         count_num = count_num + 1
77
78     end if
79 end do
80 end do
81 end do
82     r_list (round_loop, r) = r_list (round_loop, r)/count_num
83 end do
84 end do
85
86 do r = 1, ( lattice_size - 1)/2
87     find_r(r) = 0
88     do round_loop = 1, num_round
89         find_r(r) = find_r(r) + r_list (round_loop, r)
90     end do
91     find_r(r) = find_r(r)/num_round
92 end do
93
94 return
95 end function find_r
96
97 end module two_point_corr

```

## CURRICULUM VITAE

**NAME:** Jakapat Kannika **GENDER:** Male

**NATIONALITY:** Thai **DATE OF BIRTH:** October 7, 1990

**EDUCATIONS:** B.Eng. (Computer Engineering), Suranaree university of Technology,  
Thailand, 2013

**PUBLICATIONS:** -

